NASA TECHNICAL MEMORANDUM 101562

EVALUATION OF THE SPLIT CANTILEVER BEAM FOR MODE III DELAMINATION TESTING

Roderick H. Martin

(NASA-TM-101562) EVALUATION OF THE SPLIT CANTILEVER BEAM FOR MODE 3 DELAMINATION TESTING (NASA. Langley Research Center) 59 p CSCL 20K
N89-22132
Unclas
G3/39 0199122

March 1989

National Aeronautics and
Space Administration

Langley Research Center
Hampton, Virginia 23665-5225

SUMMARY

A test rig for testing a thick split cantilever beam for scissoring delamination (mode III) fracture toughness was developed. A 3-D finite element analysis was conducted on the test specimen to determine the strain energy release rate, G, distribution along the delamination front. The virtual crack closure technique was used to calculate the G components resulting from interlaminar tension, G_I, interlaminar sliding shear, G_{II}, and interlaminar tearing shear, G_{III}. The finite element analysis showed that at the delamination front no G_I component existed, but a G_{II} component was present in addition to a G_{III} component. Furthermore, near the free edges, the G_{II} component was significantly higher than the G_{III} component. The G_{II}/G_{III} ratio was found to increase with delamination length but was insensitive to the beam depth. The presence of G_{II} at the delamination front was verified experimentally by examination of the failure surfaces. At the center of the beam, where the failure was in mode III, there was significant fiber bridging. However, at the edges of the beam where the failure was in mode II, there was no fiber bridging and mode II shear hackles were observed. Therefore, it was concluded that the split cantilever beam configuration does not represent a pure mode III test. The experimental work showed that the mode II fracture toughness, G_{IIc}, must be less than the mode III fracture toughness, G_{IIIc}. Therefore, a

conservative approach to characterizing mode III delamination is to equate G_{IIIc} to G_{IIc}.

INTRODUCTION

With the increased use of laminated fiber reinforced plastics in primary aircraft structural components, the need to understand and predict the failure modes of these components has also increased. There have been many studies over the last decade examining delamination failure of composite materials and structures [1-20]. A delamination may result from high interlaminar stresses causing adjacent plies to come apart. These high stresses are caused by material and geometric discontinuites in the component, and can be tensile, compressive or shear in nature. Much work has been published on characterizing mode I (opening or peel) [1-8] and mode II (sliding or interlaminar shear) [7-15] delamination. Emphasis was initially placed on mode I fracture testing because it was the most critical mode of fracture with brittle matrix systems [8,15]. Tougher matrix systems resulted in a decreased difference between the mode I and mode II fracture toughnesses [14,15]. Mode I and mode II delamination tests are now sufficiently advanced for the various standards organizations, such as ASTM, to consider. Many delamination problems considered were found to delaminate in a combination of mode I and II [16-18]. Therefore, mode III delamination characterization was largely ignored. However, the importance of mode III delamination is beginning to be appreciated. With the complex loads seen in service, and for certain laminate configurations [19,20], mode III delamination may occur. Therefore, mode III delamination needs to be characterized.

In the present literature there are only a few suggested test methods available for characterizing mode III delamination in composite materials. Donaldson [21] developed a test using a split cantilever beam (SCB) type arrangement. This arrangement consisted of a unidirectional laminate, adhesively bonded between aluminum bars to give the specimen torsional stiffness as the delamination grew, fig 1a. The load was applied by thick metal plates bolted to the aluminum bars. The plates were pinned to the jaw of the test machine. The thick plates helped reduce the mode I delamination. The test appeared to work successfully for a brittle graphite/epoxy, but the aluminum bars debonded when a tougher thermoplastic matrix composite was used. Chaouk [20] used a similar split beam configuration using a torsion rig to introduce the load. Donaldson and Mall have also used the SCB configuration to measure fatigue delamination growth rates [22]. Becht and Gillespie developed a double rail shear test to measure mode III fracture toughnesses [23]. This test configuration was modified by Gillespie and Becht [24] to a single cracked rail shear test, because of the difficulties in growing two delaminations at one time, fig 1b.

The rail shear configurations have very low compliances and hence accurate values of compliance and change in compliance with delamination growth are difficult to obtain. The SCB however, is sufficiently compliant to extract specimen compliances from the machine cross head displacements.

However, the problem of the adherend debonding prevents the determination of delamination fracture toughness for tougher materials. One solution to the debonding problem is to make the laminates sufficiently thick to provide their own torsional stiffness. Also, in references 21 and 22, two bolts were used to transfer the load to the specimen. The data reduction assumed that the load was applied between the center of the two bolts, which may not be entirely accurate. A possible solution to this problem, would be to load the laminate edges using a loading nose system, fig 2. However, even with these modifications it is possible that the strain energy release rate along the delamination front of the SCB is not pure mode III due to the rotation of the beam about the z-axis at the delamination front causing a mode II strain energy release rate component at the specimen edges. The presence of a mode II strain energy release rate in the SCB specimen has not previously been verified. Therefore, the purpose of this study was to determine if the SCB is suitable for characterizing mode III delamination, by performing an analysis on this configuration to determine the strain energy release rate distribution along the delamination front. Also, experiments were conducted using the modified SCB configuration. The failure surfaces were examined to determine the mode of failure.

NOMENCLATURE

a	Delamination length
a_0	Initial delamination length

C	Specimen Compliance
D	Specimen Depth
E_{11}	Tensile longitudinal modulus
F	Force
G	Total strain energy release rate
G_a	Integrated average strain energy release rate
G_b	Strain energy release rate calculated from beam theory
G_c	Critical strain energy release rate
G_g	Global strain energy release rate calculated from compliance variations
G_I	Mode I component of strain energy release rate
G_{II}	Mode II component of strain energy release rate
G_{III}	Mode III component of strain energy release rate
G_{12}	Shear modulus in the x-y plane
$G(y)$	Distribution of strain energy release rate along the y-axis
h	Beam half-thickness
I	Second moment of area
P	Applied load
u,v,w	Displacements in the x-, y-, and z-directions respectively

x,y,z	Axes
δ	Beam deflection at loading point
Δ	Length of finite element at delamination front

MATERIALS

Unidirectional, 100 ply, glass/epoxy (S2/SP250) panels were manufactured at NASA Langley Research Center according to manufacturer's instructions. To simulate a 127mm (5 in.) long initial delamination, a folded 0.0127mm (0.5 mil) Kapton film was inserted between the 50th and 51st ply prior to curing. The average volume fraction for the material used was 64.6 percent. The volume fraction was determined using ASTM procedure D-3171. The specimens were manufactured to the dimensions given in figure 2.

The glass/epoxy material properties for use in the finite element analysis and beam theory expressions were obtained from reference [18] and are given in table 1. A finite element analysis was also conducted using a graphite/epoxy (AS4/3501-6) and a graphite/epoxy-aluminum alloy combination, the latter being similar to that used in reference 21. The material properties of the graphite/epoxy were taken from reference 25 and the material properties of a typical aluminum alloy were taken from reference 26 and are given in table 1. For both composites, the out-of-plane material properties were equated to the in-plane material properties for use in the 3-D finite element analysis, that is, $E_{33} = E_{22}$, $G_{13} = G_{23} = G_{12}$ and $\nu_{13} = \nu_{23} = \nu_{12}$.

TEST PROCEDURE

A test rig for simulating mode III delamination in the SCB specimens, was manufactured at NASA Langley Research Center. The test rig is shown schematically in fig. 3. The plunger was free to move vertically up and down, but was restrained from movement in any other directions. The lower reaction nose was fixed to the face plate. The face plates aided in restraining any beam rotation about the x-axis in order to suppress any mode I opening that might occur. Figure 4 shows the test rig assembled in the testing machine.

Several beams were tested at various initial delamination lengths. Initial delamination length was varied by altering the position of the beam in the test rig prior to testing. The sides of the beam were graduated in 2.5mm (0.1 in.) intervals to aid in the measurement of delamination length on the edge of the beam. Delamination initiation and propagation were observed visually, on both edges, using a low powered microscope. The tests were run under displacement control at a cross head displacement rate of 0.5 mm/minute (0.02 in./minute). The resulting load-displacement plot was recorded on an X-Y plotter. Initiation of delamination from the insert was also observed as a deflection from the initially linear part of the load-displacement plot. Further increments in delamination length were marked on the X-Y plot for subsequent data reduction. Figure 5 shows a typical load-displacement plot. For all tests, on unloading, a sudden drop in load was noticed followed by an un-smooth unloading plot. This unloading path indicates that there was friction present in the test. This friction was probably between the delaminated surfaces, and also between the face plates and the outside edges of the specimen.

ANALYSIS

Beam Theory

The compliance, C, of the SCB specimen can be determined from the deflection of a cantilever beam using elementary beam theory [27] modified for composite materials [28] in a similar way to the Double Cantilever Beam specimen (DCB) [1] thus:

$$C = \frac{\delta}{P} = \frac{2\,a^3}{3\,E_{11}\,I} + \frac{D^2\,a}{4\,G_{12}\,I} \qquad (1)$$

Equation 1 includes the contribution of transverse shear strain to deflection because of the relatively thick nature of the SCB specimens and the high E_{11}/G_{12} ratio.

The strain energy release rate, G , may be expressed as a function of the derivative of the compliance with respect to delamination length [1] thus:

$$G = \frac{P^2}{2D}\frac{dC}{da} \qquad (2)$$

Therefore, differentiating equation 1 with respect to delamination length, a , and substituting into equation 2 yields an expression for strain energy release rate thus:

$$G_b = \frac{P^2}{2D} \left(\frac{2\ a^2}{E_{11}\ I} + \frac{D^2}{4\ G_{12}\ I} \right) \tag{3}$$

However, at the delamination front of the SCB specimen, the beam theory assumption that the cantilever beam is clamped may not be valid. Any displacement in the x-direction, fig. 2, at the delamination front will cause a mode II strain energy release rate. If these displacements are present, the SCB configuration would not yield pure mode III delamination. Therefore, in order to determine the contribution of the various fracture modes to G_c, a finite element analysis was performed.

Finite Element Analysis

To evaluate the distribution of the different modes of strain energy release rate along the delamination front, a three dimensional finite element analysis (FEA) was performed using NASTRAN [29]. Two different specimen depths were considered in the analysis, D= 25.4mm (1.0in.) and D= 12.7mm (0.5in.). The model consisted of 8-node brick elements (HEXA) and 6-node wedge elements (PENTA). NASTRAN's HEXA and PENTA elements are modified isoparametric elements which use selective integration points for different components of strain. For both models the mesh was refined close to the delamination front in both the x-y plane and the x-z plane. The mesh is shown in fig. 6.

A unit line load was placed at different delamination lengths between 25.4mm and 127mm (1 and 5 ins.). No delamination lengths shorter than 25.4mm (1 in.) were considered to prevent any stress concentrations caused by the loading nose from encroaching on the delamination area. These asymmetrical loadings, fig. 2, caused the model to twist about the x-axis. This rotation was prevented by restraining the outsides of the beam in the z-direction. The restraints ran from the end of the beam to one inch ahead of the delamination front for all delamination lengths considered. These restraints also prevented any mode I opening of the SCB.

Strain energy release rate components were calculated using the 3-D Virtual Crack Closure Technique (VCCT) [30], which assumes that the work done to close the delamination by one element length is equivalent to the strain energy released when the delamination grows by one element length. Therefore, at node H in fig. 7 the component strain energy release rates can be evaluated from

$$G_I = \frac{1}{\Delta\,(y_{i-1}+y_{i+1})}\,F_z^H\,(w^B - w^E) \tag{4a}$$

$$G_{II} = \frac{1}{\Delta\,(y_{i-1}+y_{i+1})}\,F_x^H\,(u^B - u^E) \tag{4b}$$

$$G_{III} = \frac{1}{\Delta\,(y_{i-1}+y_{i+1})} F_y^H \,(v^B - v^E) \qquad (4c)$$

where F^H is the force (in the x-, y- or z-direction) at node H, computed from the contribution of the forces of all the elements on one side of the delamination with connectivity at H. The symbols u, v and w refer to displacements in the x-, y- and z-directions respectively.

The average values of total strain energy release rate, G_a, along the delamination front, were calculated as:

$$G_a = \left[\frac{1}{D}\int_0^D G_I(y)\,dy\right] + \left[\frac{1}{D}\int_0^D G_{II}(y)\,dy\right] + \left[\frac{1}{D}\int_0^D G_{III}(y)\,dy\right] \qquad (5)$$

where G(y) is the strain energy release rate distribution along the delamination front calculated using equation 4. The values of G_a were calculated by numerical integration of the strain energy release rate distributions presented in the RESULTS section.

In addition, the total strain energy release rate was also calculated globally from the FEA by calculating the change in strain energy from one FEA run at delamination length a_i and another at delamination length a_{i+1}. The global total strain energy release rate, G_g, at $a = (a_i+a_{i+1})/2$ is:

$$G_g = \frac{1}{(a_{i+1}-a_i)\,D}\left[\frac{1}{2}(\Sigma\, P\, \delta)_{a_i} - \frac{1}{2}(\Sigma\, P\, \delta)_{a_{i+1}}\right] \qquad (6)$$

where $(\Sigma\, P\, \delta)$ is the sum of the displacements (in the loading direction) of the loaded nodes, multiplied by the applied loads.

RESULTS

Finite Element Analysis

Figures 8a and 8b show the variation of compliance, C, with delamination length, a, for D= 12.7mm and 25.4mm (0.5in. and 1in.) respectively. The correlation between beam theory (the solid line) and the FEA (open triangles) was good. The beam theory results were consistently below the FEA results because beam theory assumes that the beam is fixed at the clamped end. However, the FEA allows for the y-direction displacement experienced by the beam beyond the delamination front. An analysis where the cantilever beam assumption was replaced by a beam that is partly free and partly supported by an elastic foundation, similar to that conducted for the DCB [31], may yield closer comparison between beam theory and FEA. Also shown in figs. 8a and 8b are the compliance values calculated from the experimental tests, open squares. The experimental results are discussed under the next sub-heading.

Figure 9a shows the total strain energy release rate for D= 12.7mm (0.5in) calculated three different ways; (1) by beam theory, equation 3, (solid line); (2) by the integrated average method, equation 5, (open squares); and (3) by the global method, equation 6, (open triangles). Figure 9b shows similar results for D= 25.4mm (1.0in.). Results using equation 5 and 6 yielded good agreement in the values of G/P^2. The beam theory results using equation 3 were consistently below the FEA results. This difference may again be caused by the differences noted in the determination of compliance.

Figures 10a and 10b show the distribution of the normalized mode III component of strain energy release rate, G_{III}/P^2 , along the delamination front for D= 12.7mm and 25.4mm (0.5in. and 1in.) respectively. Only half the delamination front has been plotted, because the distribution was symmetrical about the x-z plane. For all delamination lengths, the mode III component was virtually constant along the entire delamination front, but increased at the free edges.

Figures 11a and 11b show the distribution of the normalized mode II component of strain energy release rate, G_{II}/P^2 , along the delamination front for D= 12.7mm and 25.4mm (0.5in. and 1in.) respectively. Again, only half the delamination front has been plotted because the distribution was symmetrical about the x-z plane. The mode II component increased from zero at the center of the beam to a maximum at the free edge. The mode I component was nearly zero in all cases because of the restraints set on the model.

Figures 12a and 12b show the mode II and mode III components of strain energy release rate, plotted at a delamination length of 127mm (5 ins.) for D= 12.7mm and 25.4mm (0.5in. and 1in.) respectively. Along approximately half the delamination front, G_{II}/P^2 is much larger than G_{III}/P^2. At the free edge the value of G_{II}/P^2 was approximately six times the value of G_{III}/P^2 for both depths, considered.

Figures 13a and 13b show the mode II and mode III components together at a delamination length of 25mm (1in.) at D= 12.7mm and 25.4mm (0.5in. and 1in.) respectively. For a= 25mm (1in.), the mode II component was only larger than the mode III component for approximately 15 percent of the delamination front. At the free edge the G_{II}/P^2 value was approximately 3.5 times the G_{III}/P^2 value. It was concluded from figs. 12 and 13 that the G_{II}/G_{III} ratio along the delamination front was influenced by the delamination length; the larger the delamination length the greater the proportion of G_{II} along the delamination front. It was also concluded from figs. 12 and 13 that the G_{II} and G_{III} distribution was largely insensitive to the beam depth. However, for all delamination lengths considered, the mode II component was larger than the mode III component at the free edge.

To identify the effects of material on the G_{II}/G_{III} distribution, the finite element analyses were performed for a graphite/epoxy (AS4/3501-6) SCB and a combination of aluminum alloy and graphite/epoxy SCB, the latter being similar to that used in reference 21. Figures 14a and 14b show the results for a 12.7mm (0.5 in.) depth, all graphite/epoxy beam, at delamination lengths of 127mm and 25.4mm (5 ins. and 1 in.) respectively. Figs. 15a and 15b show the results for a 12.7mm (0.5 in.) depth aluminum-graphite/epoxy beam at delamination lengths of 127mm and 25.4mm (5ins. and 1in.) respectively. For both the cases studied, the G_{II}/P^2 component was larger than the G_{III}/P^2 component at the edge of the beam for either delamination length. These results were virtually identical to the glass/epoxy beams. Therefore, the distribution of G_{II} and G_{III} along the delamination front for a SCB specimen was not strongly dependent on the material system used.

Experimental

Figure 16 shows a plot of critical strain energy release rate G_c against delamination length for one of the S2/SP250 beams tested. The term G_c rather than G_{IIIc} has been used, because the results of the finite element analysis showed that delamination would not be by pure mode III alone. The quantity G_c was calculated using the beam theory expression given in equation 3. The delamination length was taken as that observed at the edge of the beam. In reality the delamination front was probably not straight, after growth from the insert, but either "U" or "V" shaped due to the variation of G_{II} along the delamination front. No account for the change in shape of the delamination front with delamination extension was taken in fig. 16. An increase in G_c was observed with an increase in delamination length. This apparent increase in G_c or "R-curve" can be attributed to fibers bridging the delaminated halves of the beam. This R-curve effect is analogous to that seen in the DCB tests using this material [6]. Observation of the delaminated halves of the beams, fig. 17, shows fiber bridging occurring in the center of the beam only. The longer the initial delamination length, the less widespread the fiber bridging along the delamination front, fig. 18. Close examination of the failure surface of the specimen, fig. 19, using a scanning electron microscope, shows the familiar shear hackles at the edge of the specimen caused by mode II failure of brittle composites [9,10,14,15]. Whereas at the center of the specimen, tangled fibers are visible. This phenomena was consistent with figures 12 and 13, which show a large mode II component near the free edges of the SCB. Therefore, figures 17 to 19 are further evidence that the SCB test has mode II failures at the outer edges of the beam.

A possible cause for fiber bridging observed in the interior of the SCB specimens is the high τ_{yz} stresses in the planes perpendicular to the fibers. These stresses may cause tensile damage in the form of micro-cracks ahead of the delamination, shown schematically in fig. 20. The damage ahead of the delamination front could cause the delamination to grow by joining the ends of the micro-cracks. When the delamination grows and connects different ends of the micro-cracks then fibers may bridge.

Fiber bridging results in a decrease of experimentally measured compliance. However, at the point of failure at the thin insert, there is no fiber bridging and the delamination front is straight. Therefore, this may be a valid value of compliance to compare with the finite element analysis. Figures 8a and 8b, show the experimental values of compliance determined at the insert for different initial delamination lengths, a_0, compared with the finite element and beam theory results. The experimental results were higher than both FEA results and the beam theory results in most cases. The difference between experimental and theoretical results may possibly be caused by the value of moduli used in the theory. The flexural moduli may be significantly lower than the tensile moduli [32], the latter being used in the analysis presented here. A decrease in the values of E_{11} and G_{12} in the analysis would increase the values of compliance as calculated from equation 1. Furthermore, compliance was calculated using cross head displacements; no correction was made for the machine compliance. Any machine deflection would result in increasing the measured compliance. In contrast, the friction observed during the experimental work, would result in reducing the measured compliance. Therefore, the differences between the experimental and analytical values of compliance have not been accounted for at this time.

For initial delamination propagation from the insert, there is no fiber bridging; therefore, an accurate and conservative value of G_c may be determined [6]. However, the FEA results showed that the longer the initial delamination length, the larger the mode II distribution along the delamination front. Figure 21 shows a plot of G_c versus initial delamination length, a_0, where G_c was calculated from delamination initiation from the insert using equation 3. A marked decrease in G_c with initial delamination length was observed for both specimen depths considered. Generally, the 25mm (1 in.) depth specimens had a higher G_c value than the 12.7mm (0.5 in.) depth. This result was possibly due to the increased friction caused by the larger surface area. Figure 21 is an indication that as the G_{II}/G_{III} ratio increases with increased delamination length, the value of G_c for the beam decreases. Therefore, it can be concluded that $G_{IIc} < G_{IIIc}$.

The values of G_c in fig. 21 may be compared with the values of $G_{Ic} = 0.14$ N/mm (0.8lb/in.) [6] and $G_{IIc} = 1.19$ N/mm (6.8lb/in.) [15] using the same material, determined from delamination initiation from a thin insert. All the values of G_c in fig. 21 are higher than the pure mode I and mode II fracture toughnesses, because although there is a significant mode II component, there is also a mode III component along the entire delamination front. The mode III component is the predominant mode of delamination failure in the center of the beam. Therefore, the total G_c value obtained from beam theory expressions and experimental testing will always be higher than the pure mode II fracture toughness, if $G_{IIc} < G_{IIIc}$.

For material systems that may not experience as much fiber bridging, such as AS4/3501-6, different experimental results to the "R-curve" shown in fig 16 may be expected. With no fiber bridging to increase the apparent G_{IIIc} component, no increase in G_c would be seen as the delamination grew in the specimen. Instead, as the delamination length increased the mode II component, along the delamination front, increased. Thus, a decrease in experimental G_c with delamination growth may be observed [21].

DISCUSSION

If a material characterization test is to be developed, it should take the simplest form possible, to allow testing of the many different material systems for quick quality control screening. The SCB test would have represented a simple method to examine mode III fracture. However, because of the mode II contribution to failure it should not be used. Other types of mode III tests mentioned in the Introduction also have testing effects which may make them unsuitable for mode III testing. For the case of mode III delamination, the simplest methods of testing have been attempted with limited success. Other test configurations may exist. However, if the laminate is loaded in pure mode III, fiber bridging may occur. Thus, only one valid G_{IIIc} value, at the insert, will be obtained from the test. It was shown in this work that G_{IIIc} was larger than G_{IIc}. Hence, in the absence of a pure mode III test method, a conservative approach to characterizing mode III delamination, by simply equating G_{IIIc} to G_{IIc}, should be adopted.

CONCLUSIONS

This work investigated mode III delamination of composites. A test rig suitable for testing a thick, split composite beam was developed. A finite element analysis was conducted on the test specimen to determine the strain energy release rate distribution along the delamination front. The following conclusions were obtained:

1. The finite element analysis showed that at the edge of the delamination front, G_{II} was significantly higher than G_{III} for all beam depths, delamination lengths and a variety of materials considered.
2. The distribution of G_{II} and G_{III} along the delamination front was dependent on the delamination length. As the delamination length increased, the ratio of G_{II}/G_{III} along the delamination front increased.
3. The distribution of G_{II} and G_{III} along the delamination front was largely insensitive to beam depth and largely independent of the material system.
4. The distribution of G_{II} and G_{III} along the delamination front was confirmed by examination of the failed surfaces of the test specimens. Where the delamination was mode II, hackles were present and no fiber bridging was observed. Where the delamination was mode III, fiber bridging was observed.

5. Plots of G_c as a function of initial delamination length indicated that G_{IIc} was less than G_{IIIc}. Therefore, a conservative approach to characterizing mode III delamination is to equate G_{IIIc} to G_{IIc}.

ACKNOWLEDGMENTS

This work was done while the author held an NRC Research Associateship at NASA Langley Research Center. The author wishes to acknowledge the help of Dr. S.A. Salpekar of Analytical Services and Materials, Inc. and Dr. T.K. O'Brien of the U.S. Army Aerostructures Directorate at Langley.

REFERENCES

1. Whitney, J.M., Browning, C.E. and Hoogsteden, W., "A Double Cantilever Beam Test for Characterizing Mode I Delamination of Composite Materials," Journal of Reinforced Plastics and Composites, Vol. 1, October 1982, pp.297-313.

2. Wilkins, D.J., Eisenmann, J.R., Camin, R.A., Margolis, W.S. and Benson, R.A., "Characterizing Delamination Growth in Graphite-Epoxy," Damage in Composite Materials, ASTM STP 775, K.L.Reifsnider Ed., 1982, pp. 168-183.

3. Russell, A.J., "Factors Affecting the Opening Mode Delamination of Graphite/Epoxy Laminates," Defence Research Establishment Pacific (DREP), Canada, Materials Report 82-Q, December 1982.

4. Carlile, D.R. and Leach, D.C., "Damage and Notched Sensitivity of Graphite/PEEK Composites," Proceedings of the 15th National SAMPE Technical Conference, October 1983, pp.82-93.

5. Keary, P.E., Ilcewicz, L.B., Shaar, C. and Trostle, J., "Mode I Interlaminar Fracture Toughness of Composite Materials Using Slender Double Cantilever Beam Specimens," Journal of Composite Materials, Vol.19, March 1985, pp.154-177.

6. Martin, R.H., "Effect of Intial Delamination on G_{Ic} and G_{Ith} Values from Glass/Epoxy Double Cantilever Beam Tests," Proceedings of the American Society for Composites, Third Technical Conference, Seattle, WA, September 25-29, 1988, pp. 688-700.

7. Martin, R.H. and Murri G.B., "Characterization of Mode I and Mode II Delamination Growth and Thresholds in Graphite/PEEK Composites," NASA TM 100577, April 1988, presented at the 9th ASTM Symposium on Composite Materials: Testing and Design, Reno, Nevada, April 1988.

8. Russell, A.J., and Street, K.N., "Factors Affecting the Interlaminar Fracture Energy of Graphite/Epoxy Laminates," in Progress in Science and Engineering of Composites, Proceedings of the Fourth International Conference on Composite Materials (ICCM-IV), Tokyo, 1982, p.279.

9. Russell, A.J., " On the Measurement of Mode II Interlaminar Fracture Energies," Defence Research Establishment Pacific (DREP) Canada, Materials Report 82-0, December, 1982.

10. Murri, G.B. and O'Brien, T.K., "Interlaminar G_{IIc} Evaluation of Toughened Resin Composites Using the End-notched Flexure Test," AIAA-85-0647, Proceedings of the 26th AIAA/ASME/ASCE/AHS Conference on Structures, Structural Dynamics and Materials, Orlando, Florida, April, 1985, p.197.

11. Mall, S. and Kochhar, N.K., "Finite Element Analysis of End Notched Flexure Specimens," J. of Composites Technology and Research, Vol. 8, No.2, Summer 1986, p.54.

12. Salpekar, S.A., Raju, I.S. and O'Brien T.K., "Strain-Energy-Release Rate Analysis of the End-notched Flexure Specimen Using the Finite-Element Method," NASA TM 100494, November 1987, Submitted to the Journal of Composites Technology and Research.

13. Carlsson, L.A., Gillespie, J.W. and Pipes, R.B., "On the Analysis and Design of the End Notched Flexure (ENF) Specimen for Mode II Testing," J. of Composite Materials, Vol.20, November, 1986, p. 594.

14. Carlsson, L.A., Gillespie, J.W. and Tretheway, B.R., "Mode II Interlaminar Fracture of Graphite/Epoxy and Graphite/PEEK", J. of Reinforced Plastics and Composites, Vol. 5, July, 1986, p.170.

15. O'Brien, T.K., Murri, G.B. and Salpekar, S.A., "Interlaminar Shear Fracture Toughness and Fatigue Thresholds for Composite Materials," NASA TM 89157, August 1987, Presented at the 2nd ASTM Symposium on <u>Composite Materials: Fatigue and Fracture</u>, Cincinnati, Ohio, April 1987. To appear in ASTM STP 1012, 1988.

16. O'Brien, T.K., "Mixed-Mode Strain-Energy-Release-Rate Effects on Edge Delamination of Composites," <u>Effects of Defects in Composite Materials</u>, ASTM STP 836, 1984, p. 125.

17. Whitcomb, J.D., "Instability-Related Delamination Growth of Embedded and Edge Delaminations," Ph.D. Thesis, Virginia Polytechnic Institute and State University, May 1988.

18. Salpekar, S.A., Raju, I.S. and O'Brien T.K., "Strain Energy Release Rate Analysis of Delamination in a Tapered Laminate Subjected to Tension Load," Proceedings of the American Society for Composites, Third Technical Conference, Seattle, WA, September 25-29, 1988, pp. 642-654.

19. O'Brien, T.K. and Raju, I.S., "Strain-Energy-Release Rate Analysis of Delamination Around an Open Hole in Composite Laminates," AIAA-84-0961, Proceedings of the 25th AIAA/ASME/ASCE/AHS Conference on Structures, California, May, 1984, p. 526-536

20. Chaouk, H., "Edge Delamination Behaviour in Advanced Composite Structures Under Compression Loading," Ph.D. Thesis, The University of Sydney, Australia, February, 1988.

21. Donaldson, S.L., "Mode III Interlaminar Fracture Characterization of Composite Materials," M.Sc. Thesis, University of Dayton, Ohio, April, 1987.

22. Donaldson, S.L. and Mall, S., "Delamination Growth in Graphite/Epoxy Composites Subjected to Mode III Loading," Journal of Reinforced Plastics. (To be published.)

23. Becht, G. and Gillespie Jr., J.W., "Design and Analysis of a Mode III Interlaminar Fracture Specimen," Composites Science and Technology, Vol. 31, 1987, p.143.

24. Gillespie Jr., J.W. and Becht, G., "An Investigation of Interlaminar Fracture of Composite Materials Under Mode III Loading", Presented at Composites '88, Boucherville, Quebec, Canada, November, 1988.

25. DOD/NASA Advanced Composites design Guide, Vol. IVa - Materials, 1st Edition, Contract No. F33615-78C-3203, Flight Dynamics Lab, Wright Patterson Air Force Base, July, 1983.

26. Dieter, G.E., "Mechanical Metallurgy," 2nd Edition, McGraw-Hill Book Co., 1976, p.51.

27. Timoshenko, S.P., "Strength of Materials, Part 1," 3rd Edition, D. Van Nostrand Co., Inc., 1955, p.170.

28. Whitney, J.M., Browning, C.E. and Mair, A., "Analysis of the Flexure Test for Laminated Composites," Composite Materials: Testing and Design (Third Conference), ASTM STP 546, 1974, p.30.

29. NASTRAN Users Manual, Version 65, Document No. MSR-39, MacNeal-Schwendler Corporation, November, 1985.

30. Shivakumar, K.N., Tan, P.W. and Newman Jr., J.C., "A Virtual Crack-Closure Technique for Calculating Stress Intensity Factors for Cracked Three Dimensional Bodies," International Journal of Fracture, Vol. 36, 1988, pp. R43-R50.

31. Kanninen, M.F., "An Augmented Double Cantilever Beam Model for Studying Crack Propagation and Arrest," International Journal of Fracture, Vol. 9, No. 1, March, 1973, pp. 83-91.

32. Zweben, C., Smith, W.S. and Wardle, M.W., "Test Methods for Fiber Tensile Strength, Composite Flexural Modulus, and Properties of Fabric-Reinforced Laminates," Composite Materials: Testing and Design (Fifth Conference), ASTM STP 674, S.W. Tsai Ed., 1979, pp. 228-262.

Table 1 Material Properties

Material	E_{11} kN/mm^2 (Msi)	E_{22} kN/mm^2 (Msi)	G_{12} kN/mm^2 (Msi)	ν_{12}
S2/SP250	43.5 (6.31)	17.2 (2.50)	4.14 (0.60)	0.25
AS4/3501-6	106.2 (15.40)	6.39 (0.927)	4.47 (0.649)	0.275
Aluminum Alloy	72.4 (10.5)	72.4 (10.5)	27.6 (4.0)	0.31

Figure 1a - Split Cantilever Beam Specimen

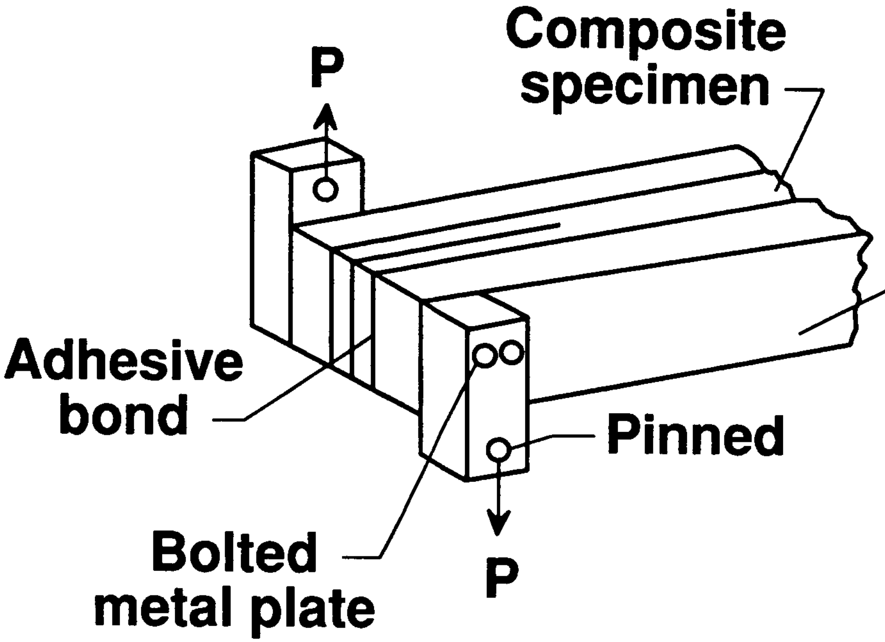

Figure 1b - Crack Rail shear Specimens

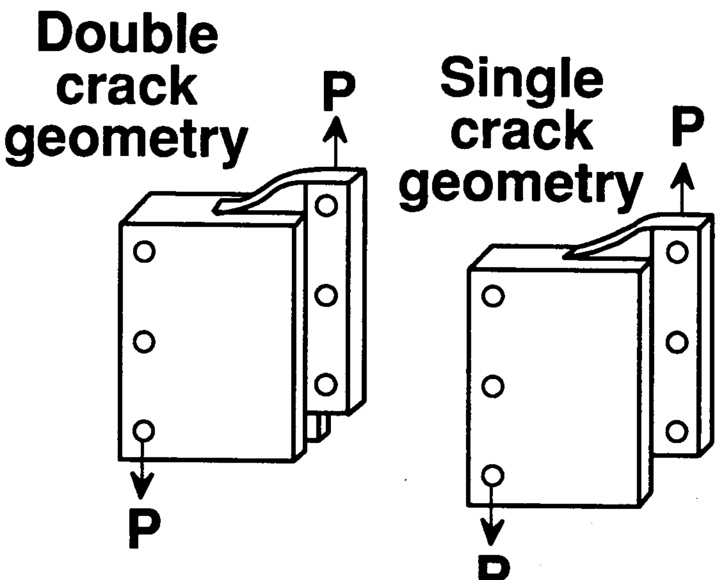

Figure 1 - Mode III Test Configurations

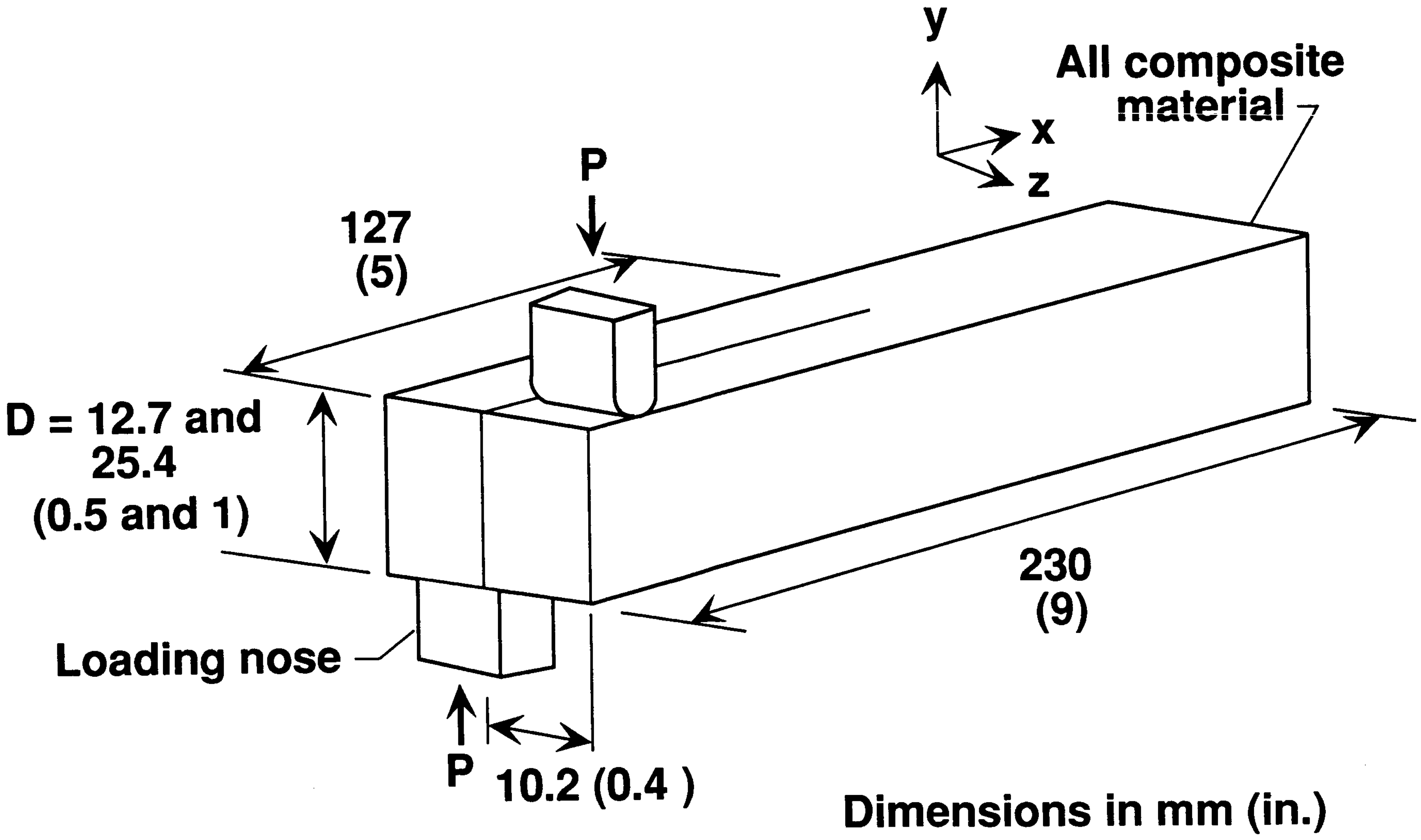

Figure 2 - Modified Split Cantilever Beam Specimen

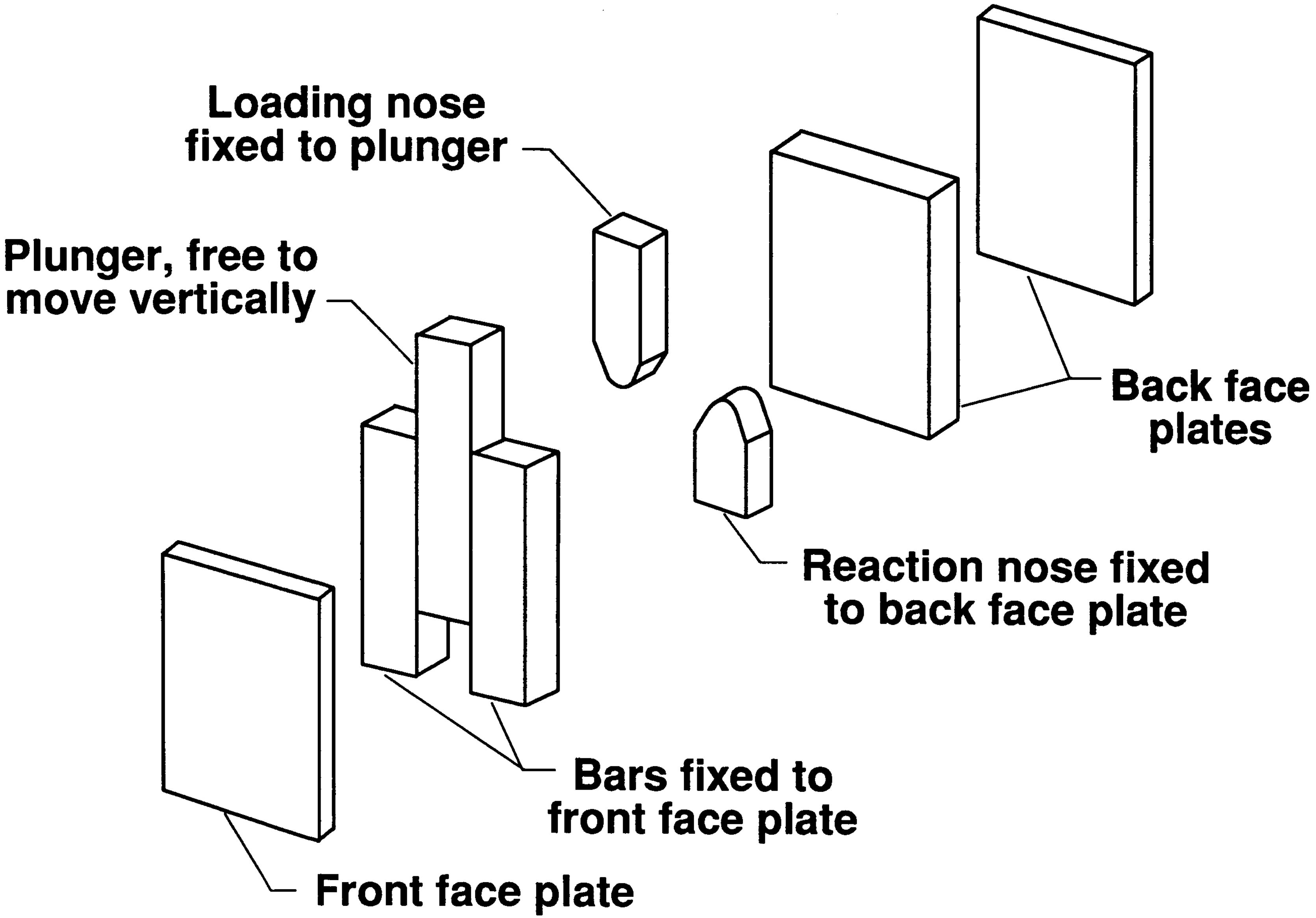

Figure 3 - Schematic of Mode III Test Rig

ORIGINAL PAGE
BLACK AND WHITE PHOTOGRAPH

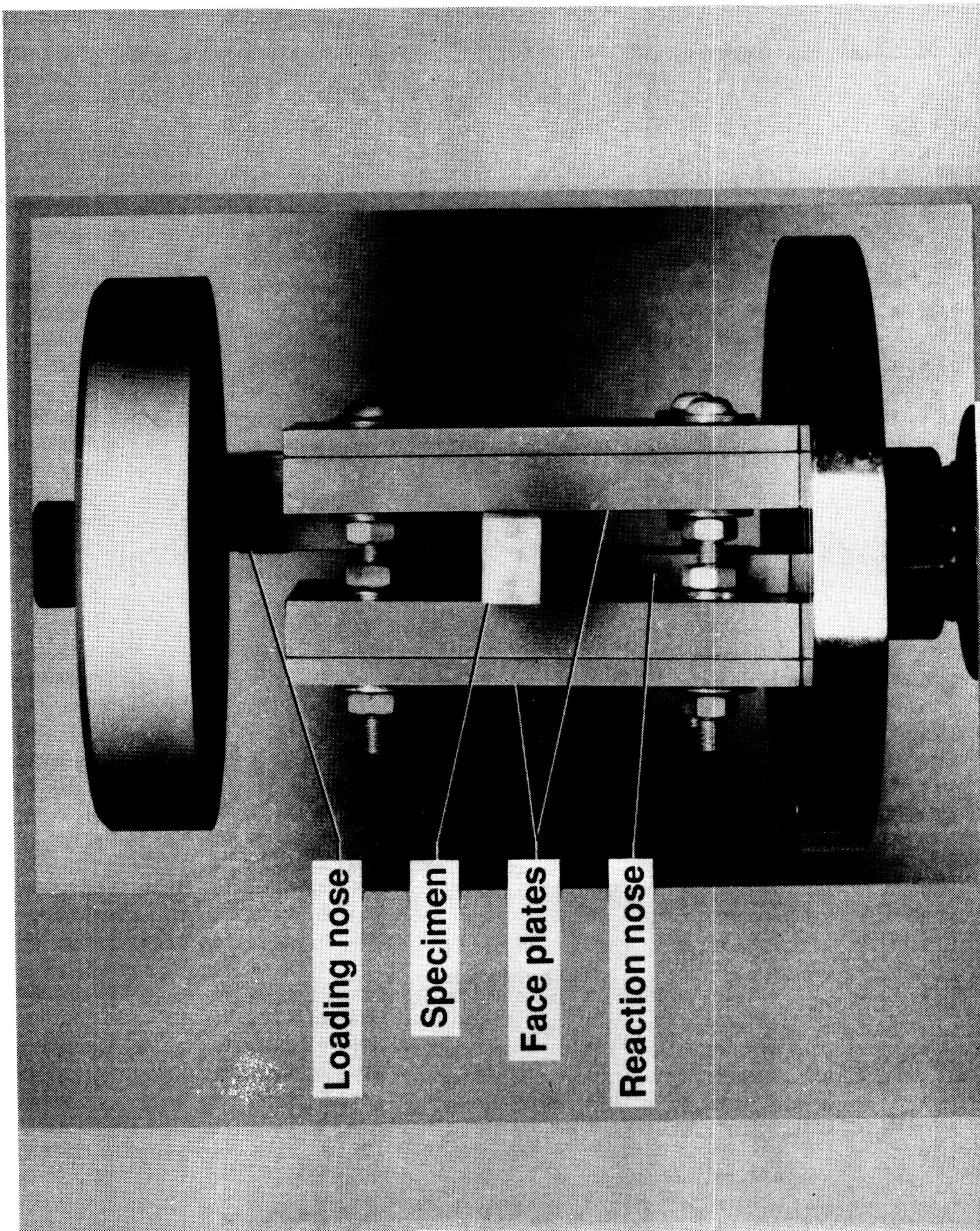

Figure 4 - Mode III Test Rig in Test Machine

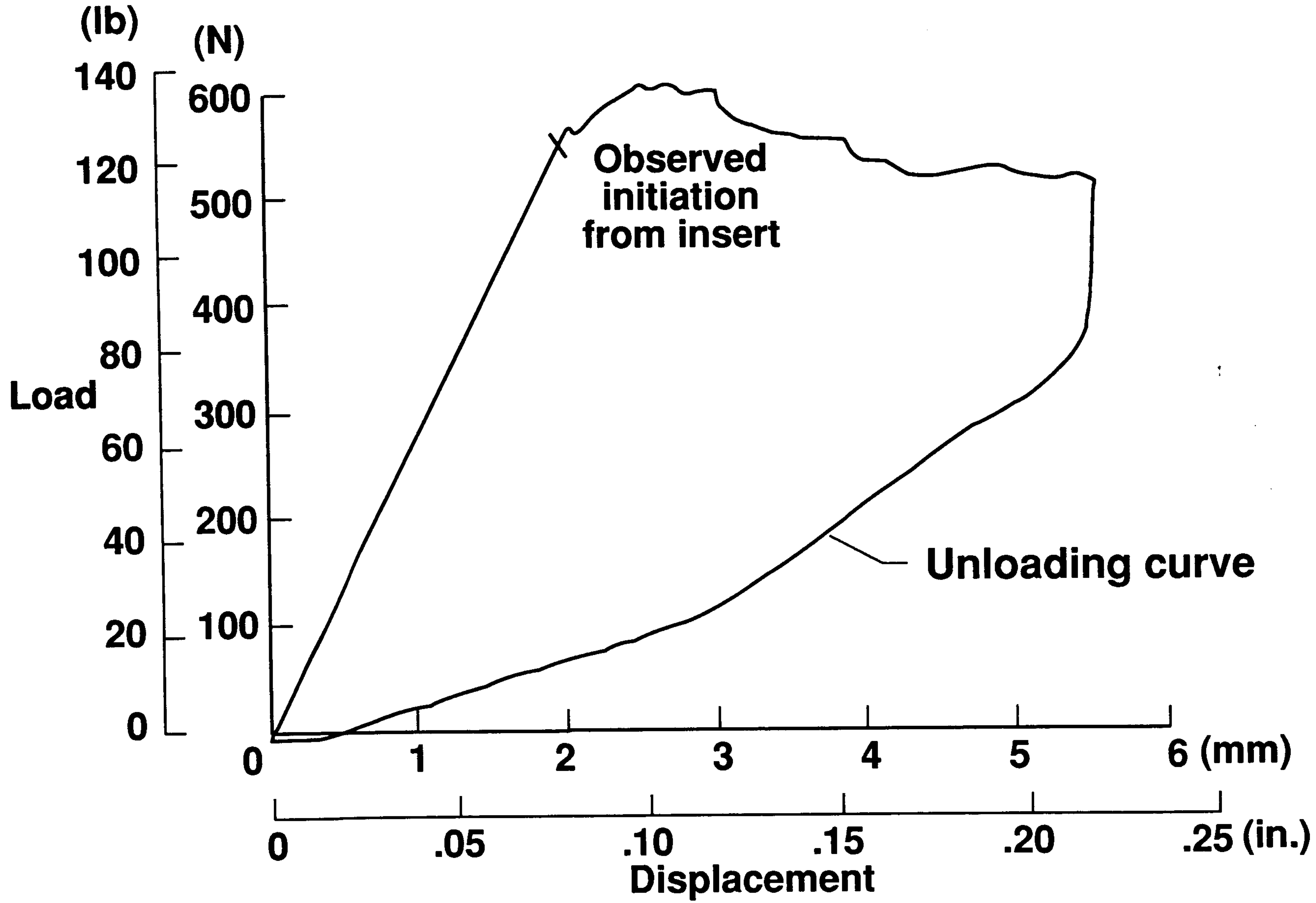

Figure 5 - Typical Mode III Load-Displacement Curve

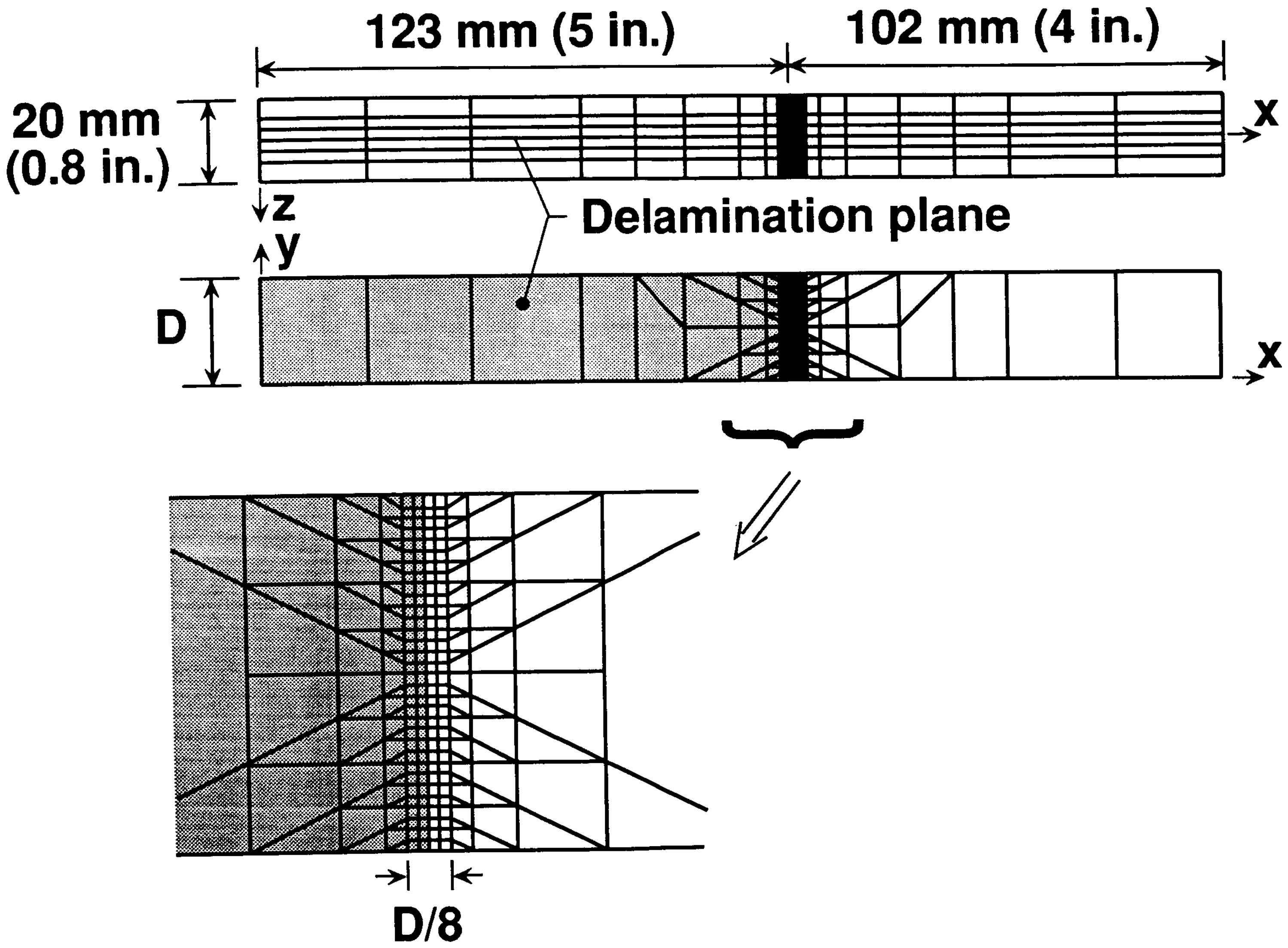

Figure 6 - Finite Element Mesh

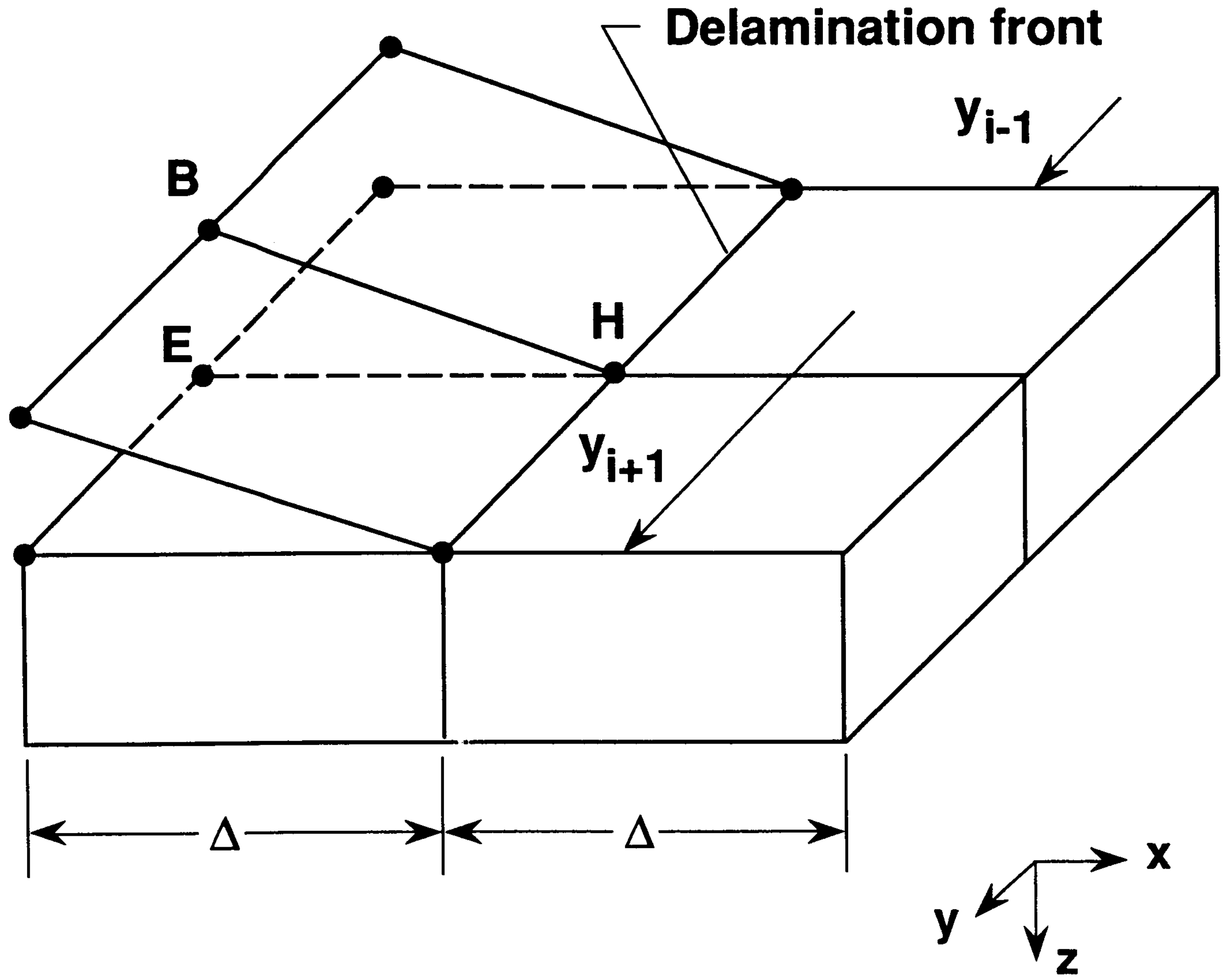

Figure 7 - Schematic of Delamination Front

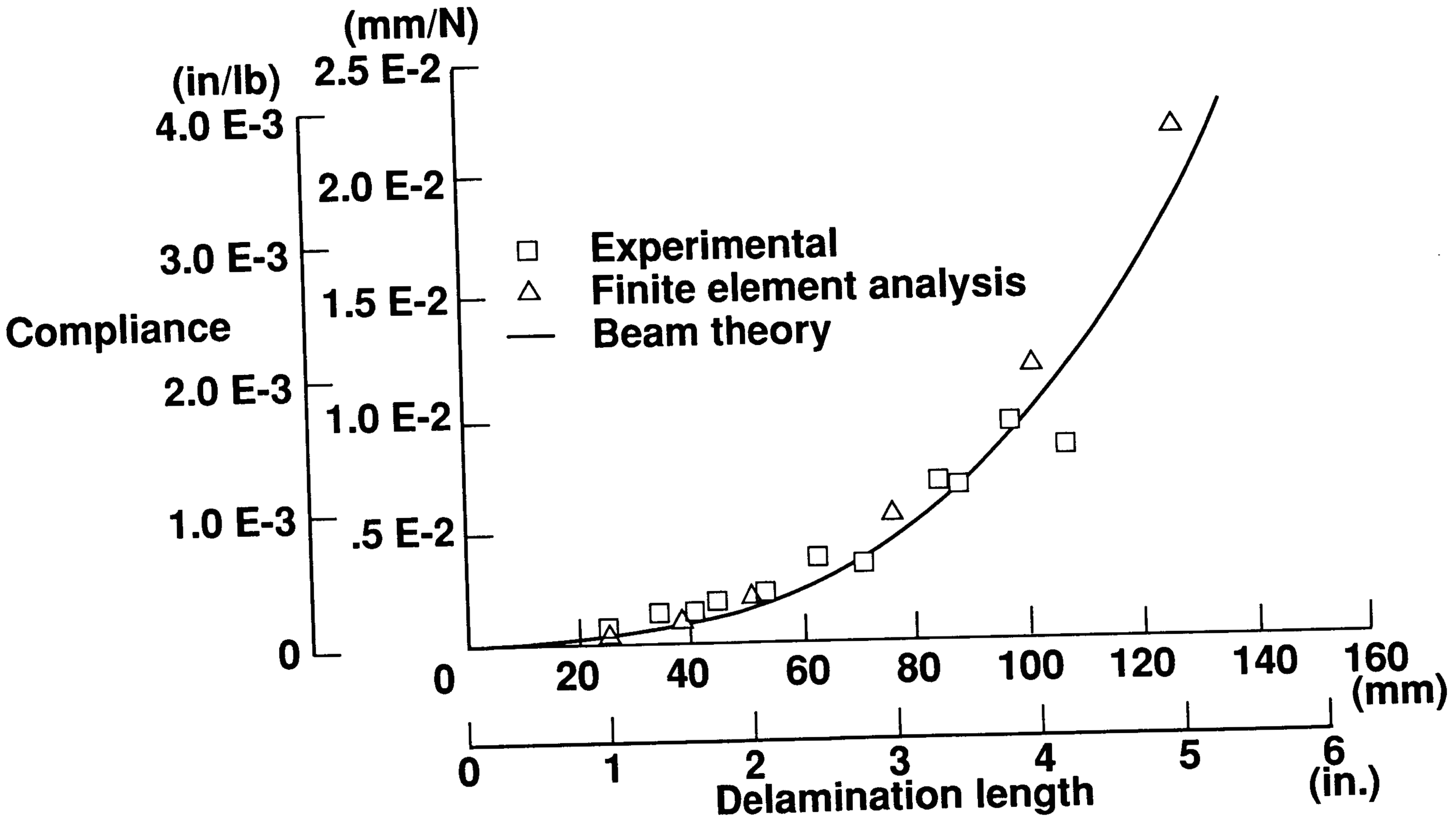

Figure 8a - Compliance Versus Delamination Length for the S2/SP250 SCB, D = 12.7 mm (0.5 in.)

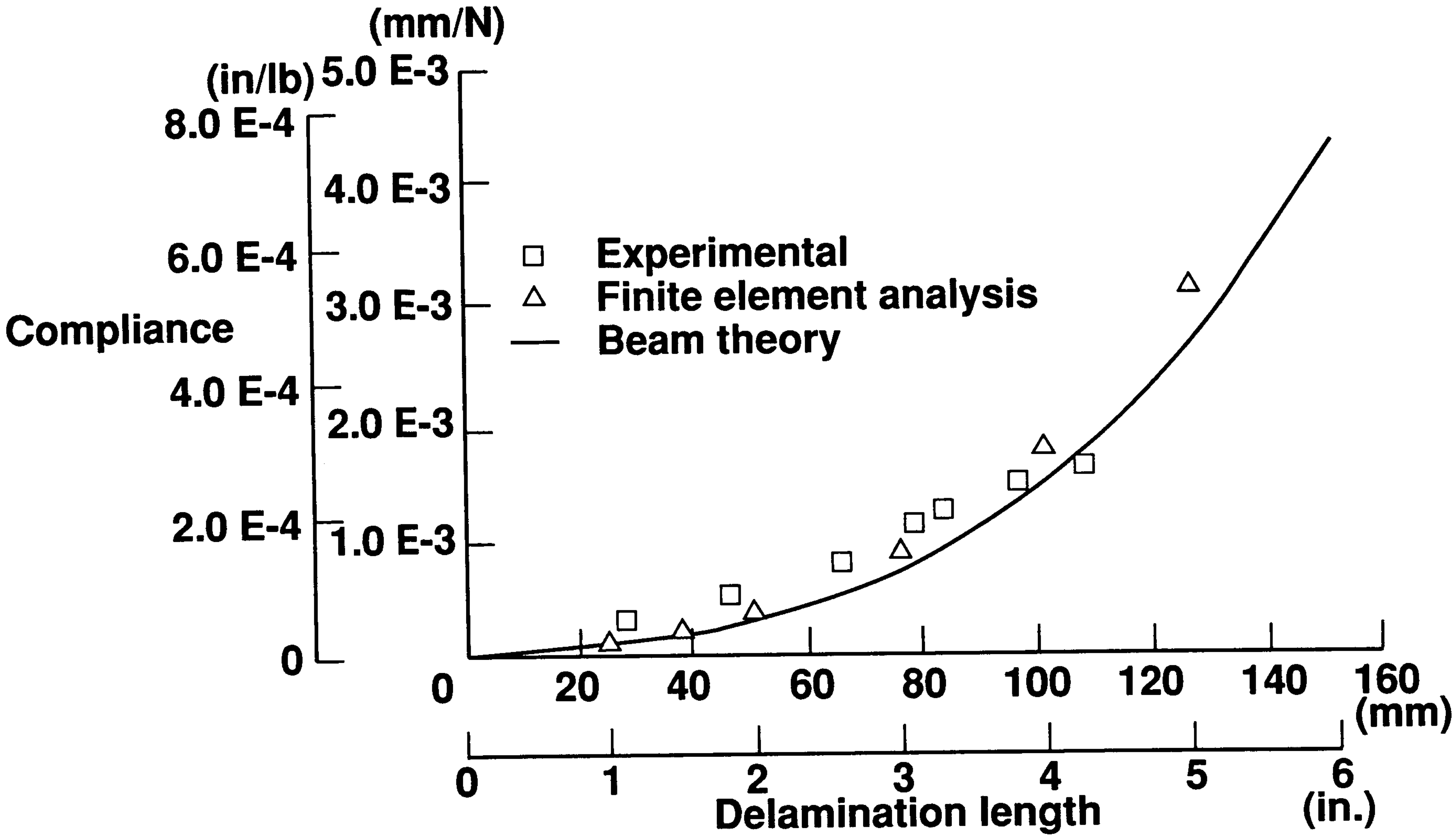

Figure 8b - Compliance Versus Delamination Length for the S2/SP250 SCB, D = 25.4 mm (1 in.)

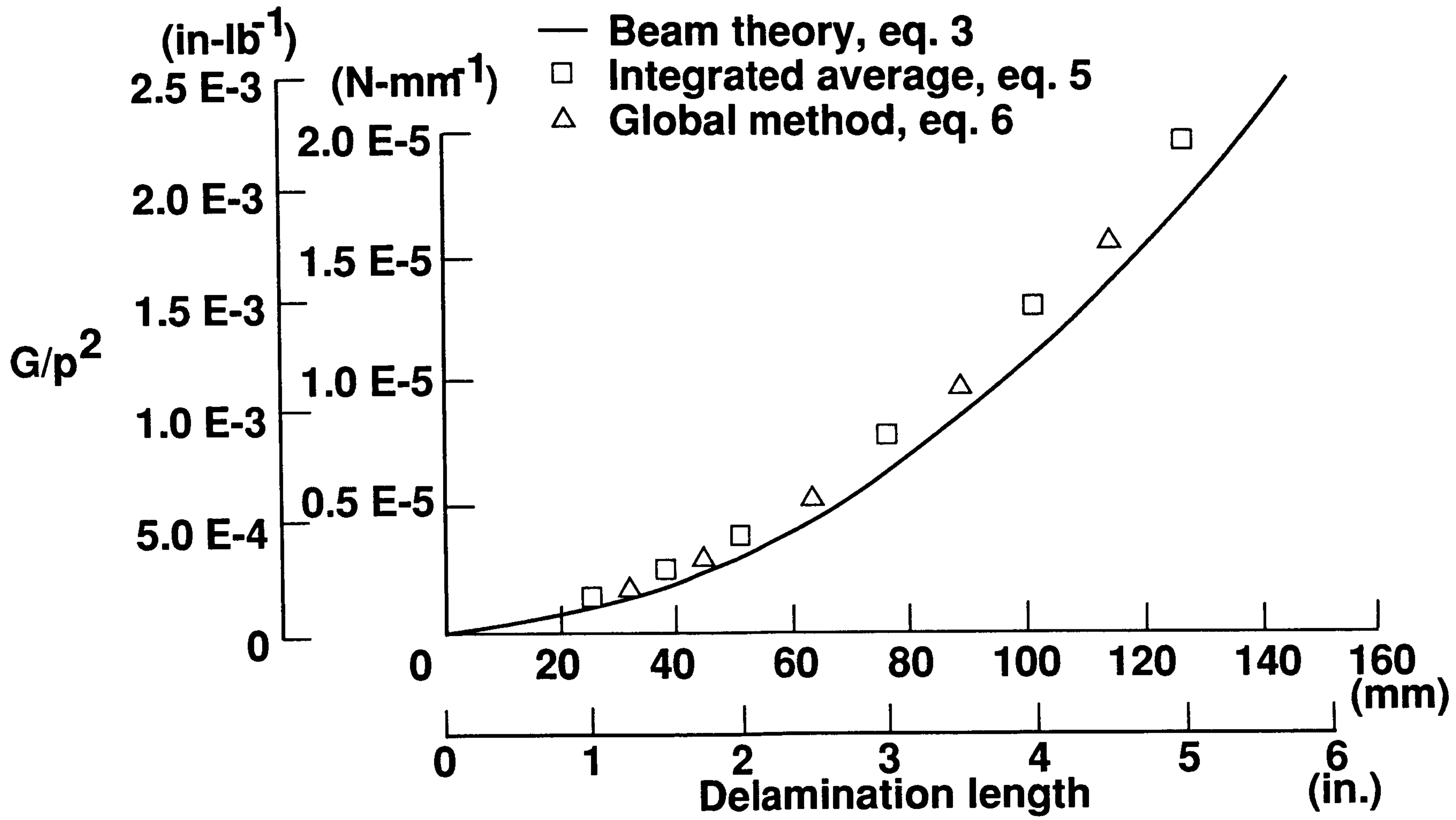

Figure 9a - Computed Strain Energy Release Rates for the S2/SP250 SCB, D = 12.7 mm (0.5 in.)

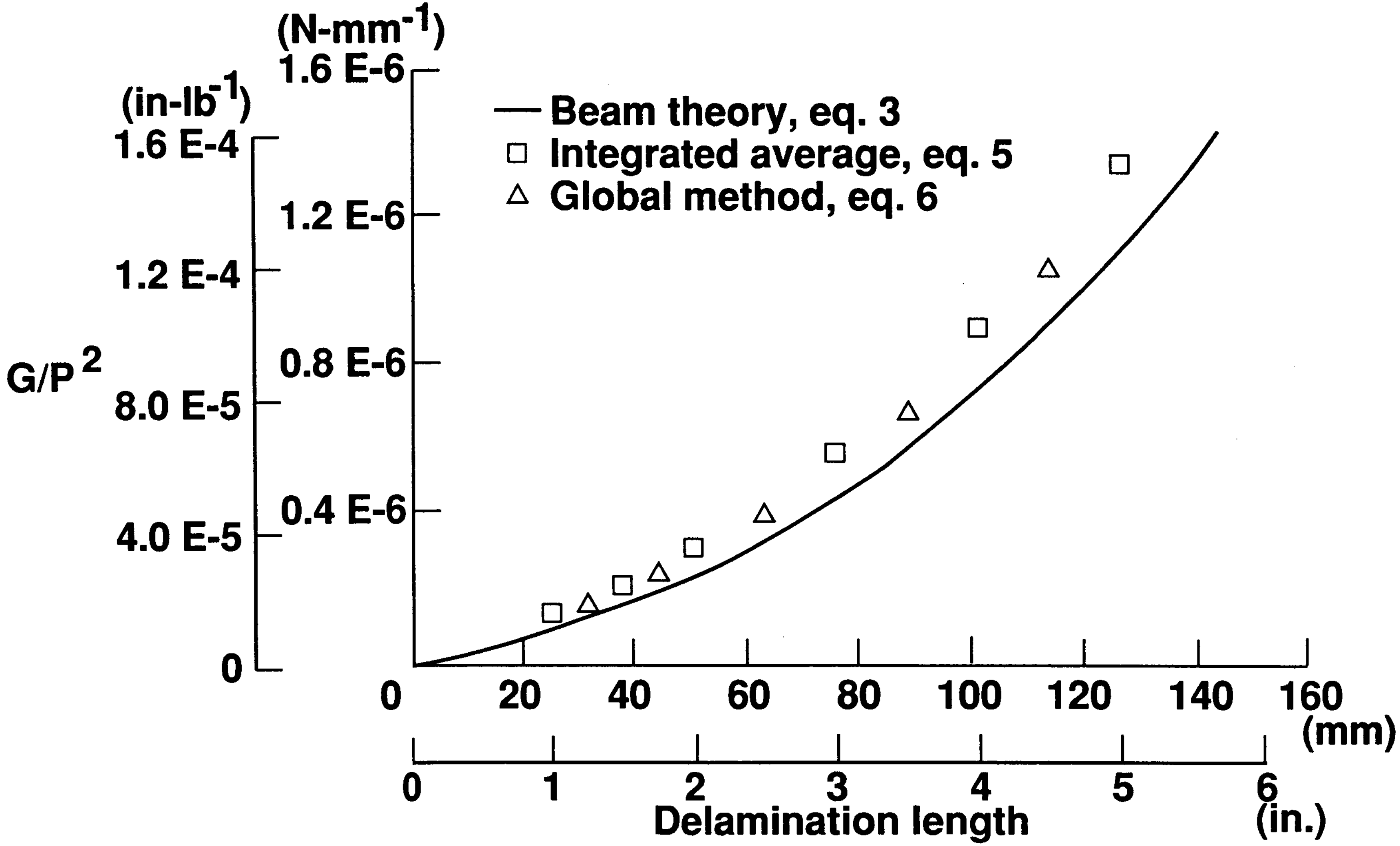

Figure 9b - Computed Strain Energy Release Rates for the S2/SP250 SCB, D = 25.4 mm (1 in.)

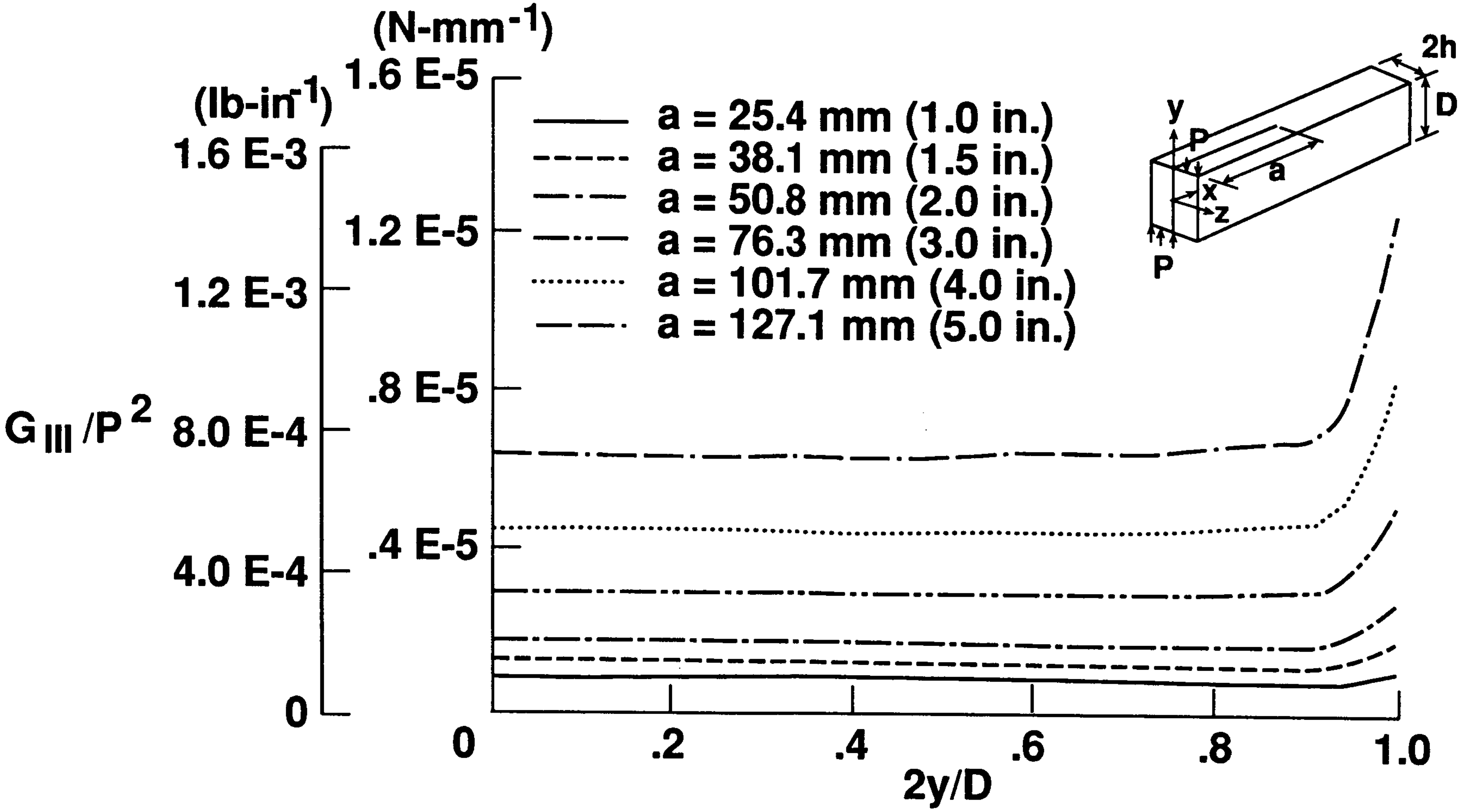

Figure 10a - G_{III} Variation Along Delamination Front, S2/SP250, D = 12.7 mm (0.5 in.)

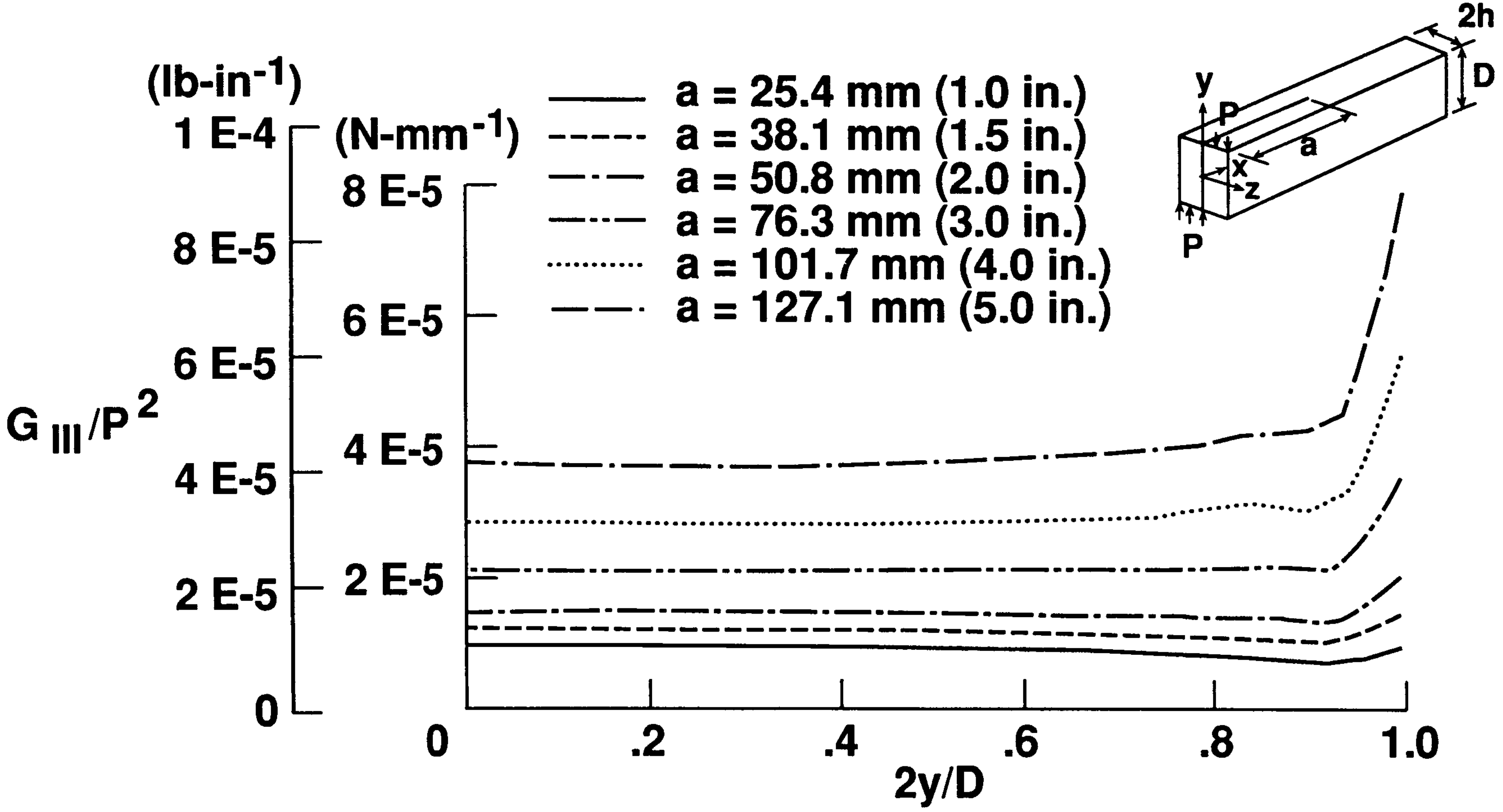

Figure 10b - G_{III} Variation Along Delamination Front, S2/SP250, D = 25.4 mm (1 in.)

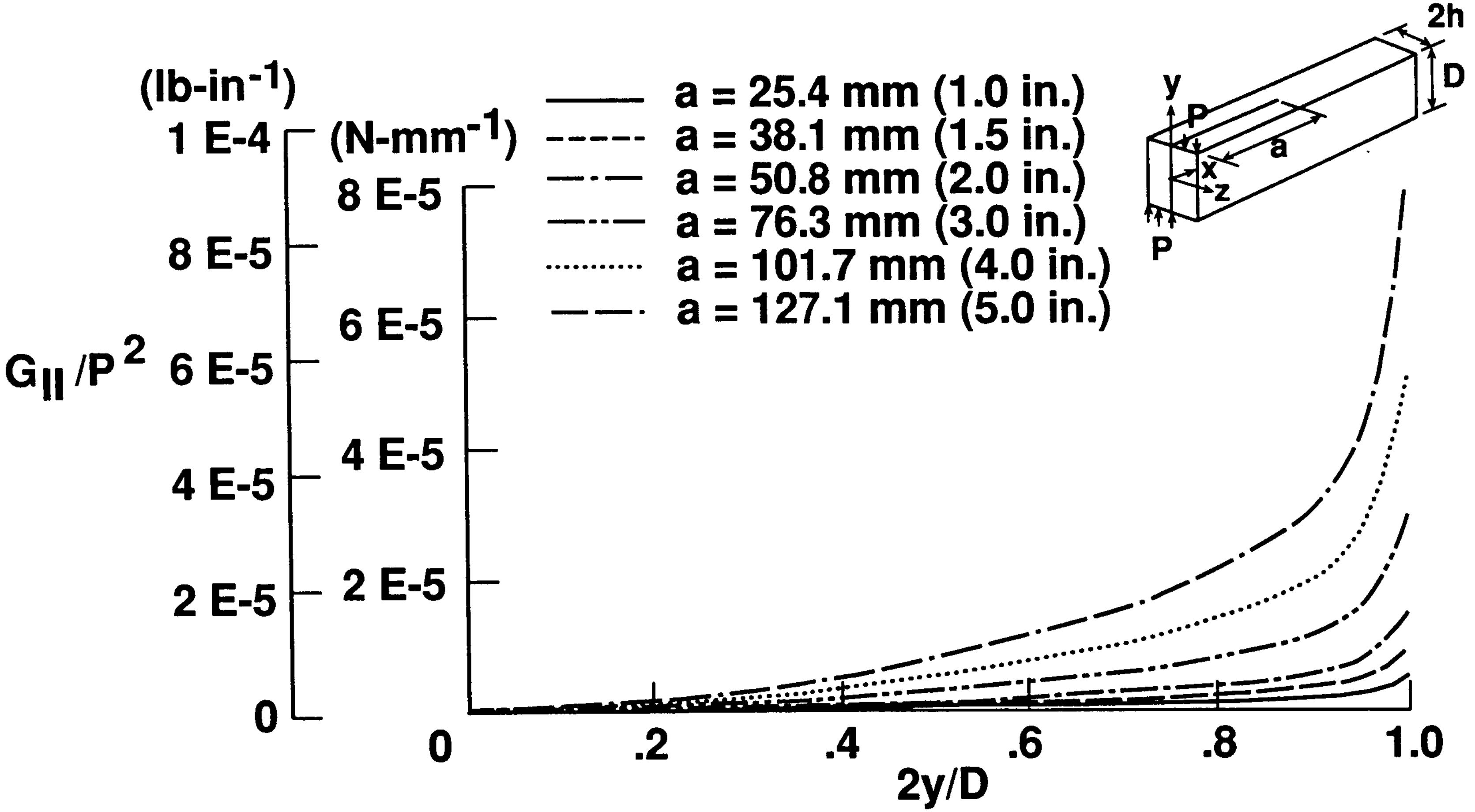

Figure 11a - G_{II} Variation Along Delamination Front, S2/SP250, D = 12.7 mm (0.5 in.)

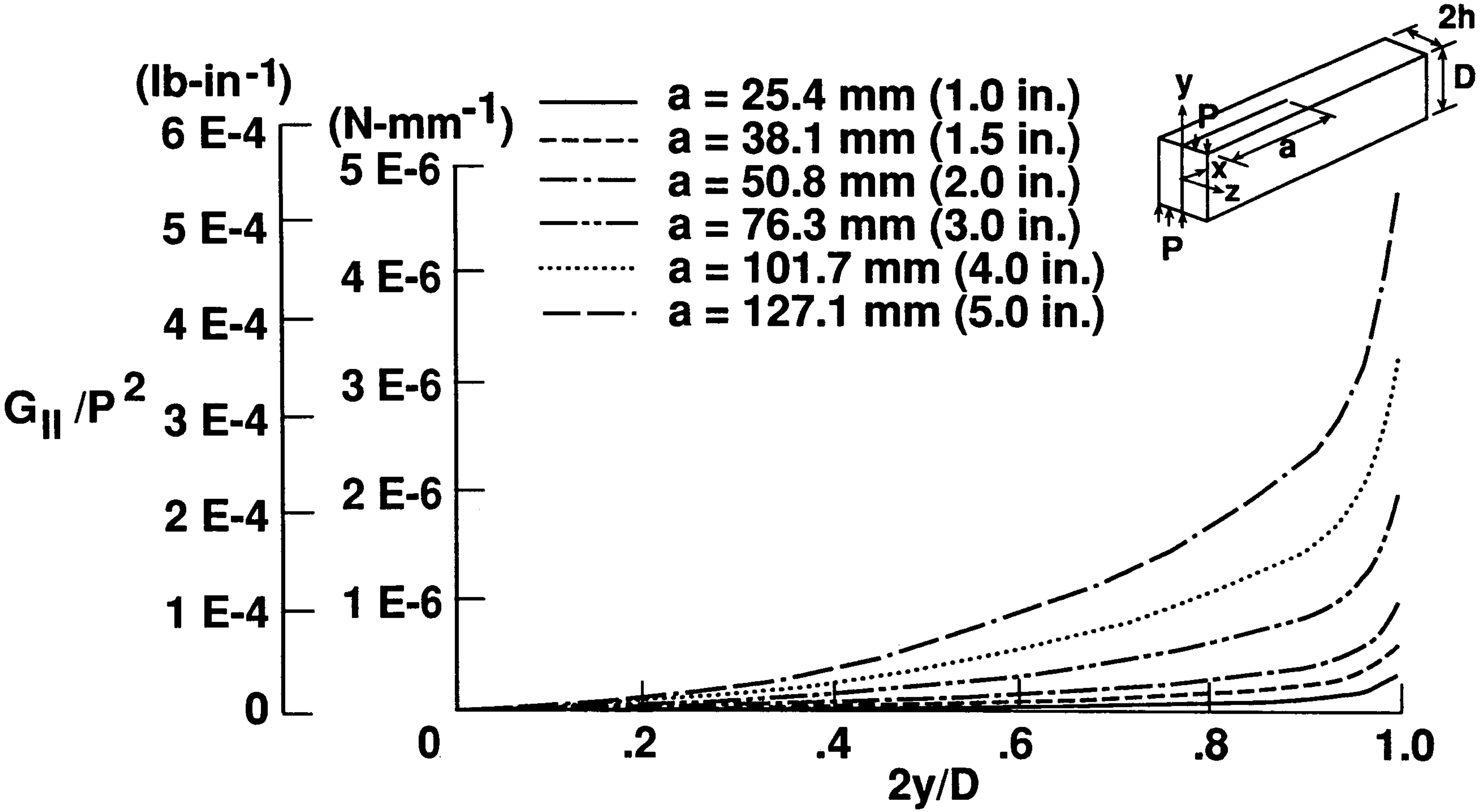

Figure 11b - G_{II} Variation Along Delamination Front, S2/SP250, D = 25.4 mm (1 in.)

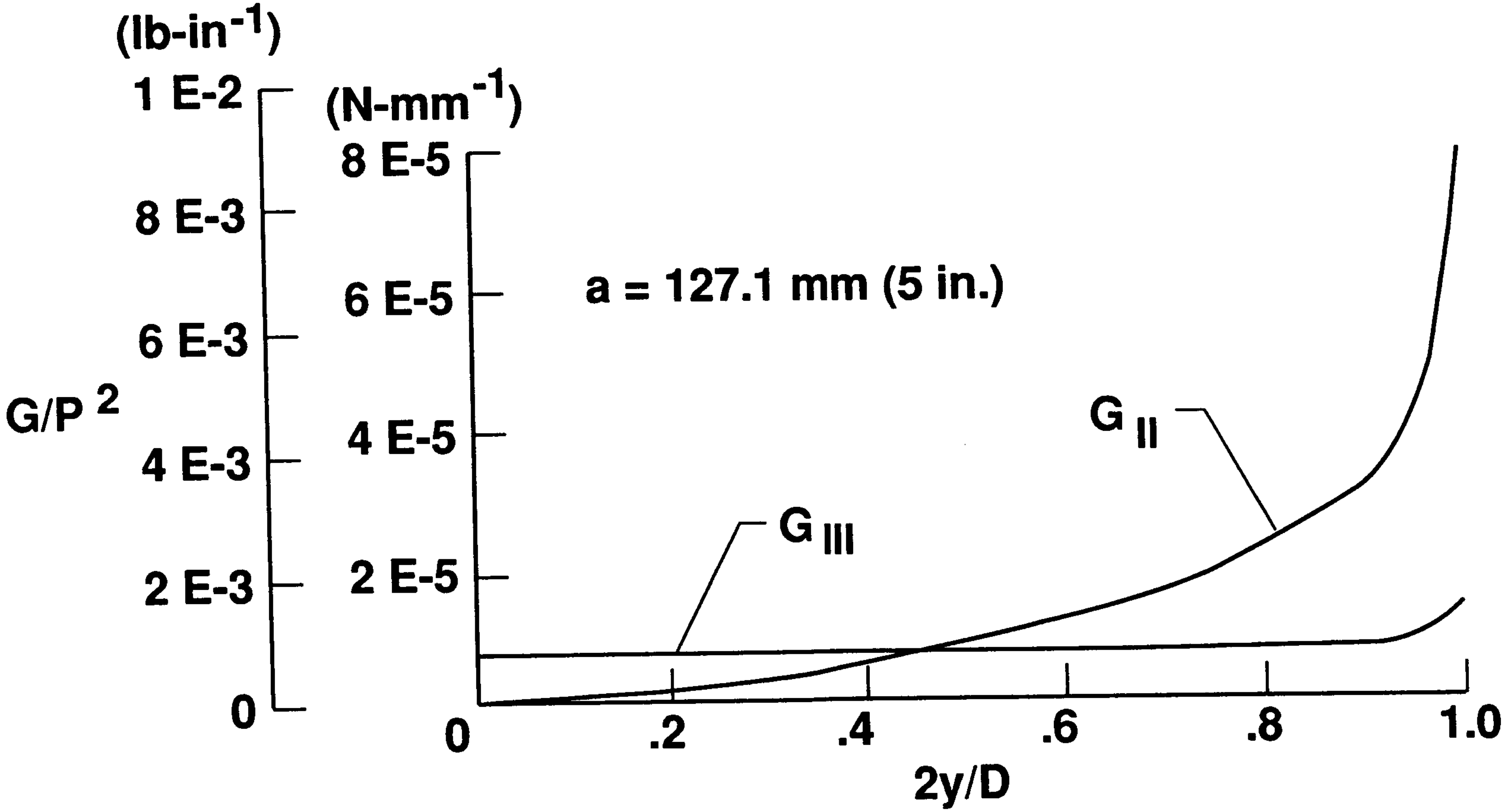

Figure 12a - G_{II} and G_{III} Distribution Along Delamination Front, S2/SP250, D = 12.7 mm (0.5 in.), a = 127.1 mm (5 in.)

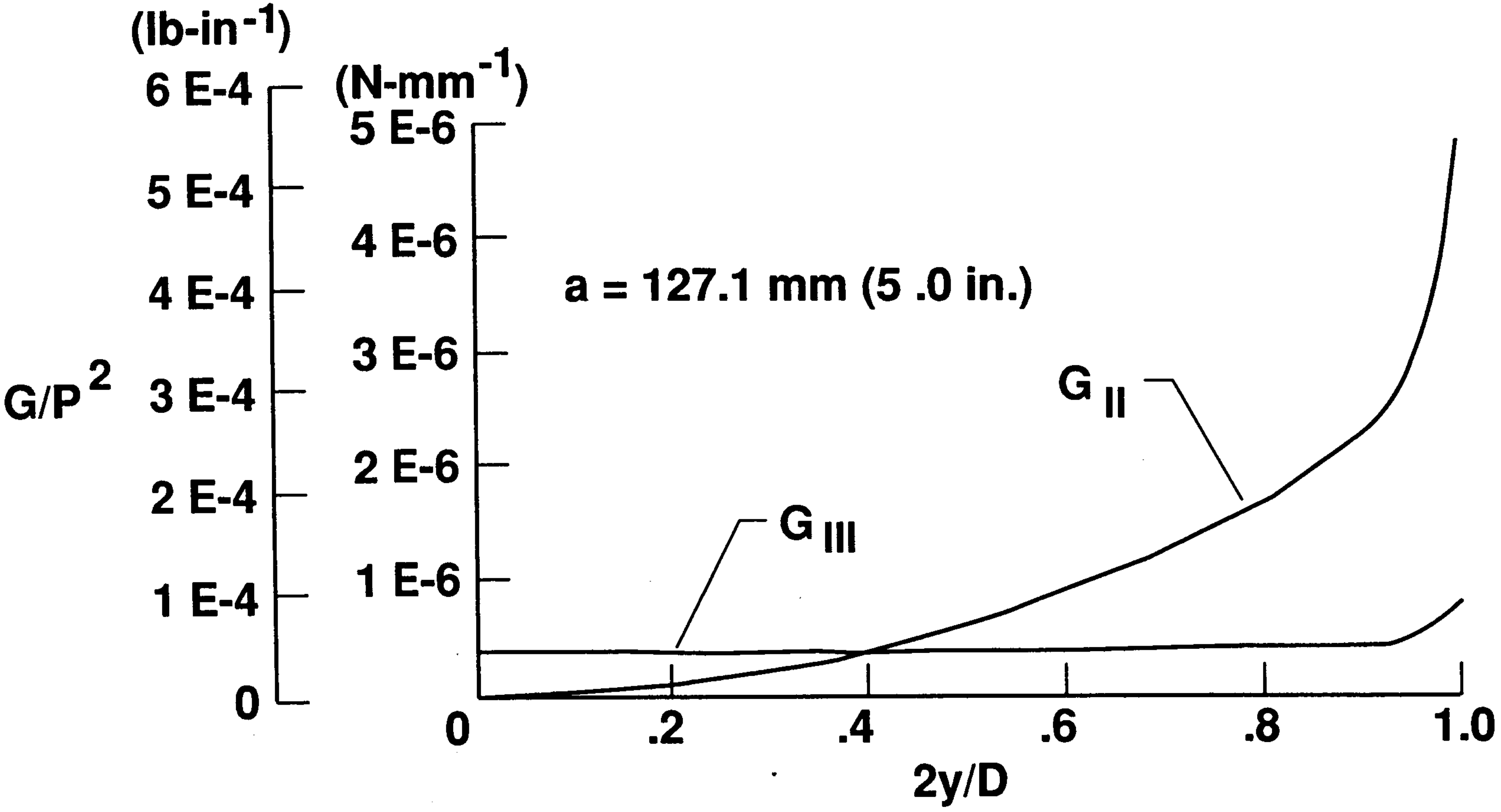

Figure 12b - G_{II} and G_{III} Distribution Along Delamination Front, S2/SP250, D = 25.4 mm (1 in.), a = 127.1 mm (5 in.)

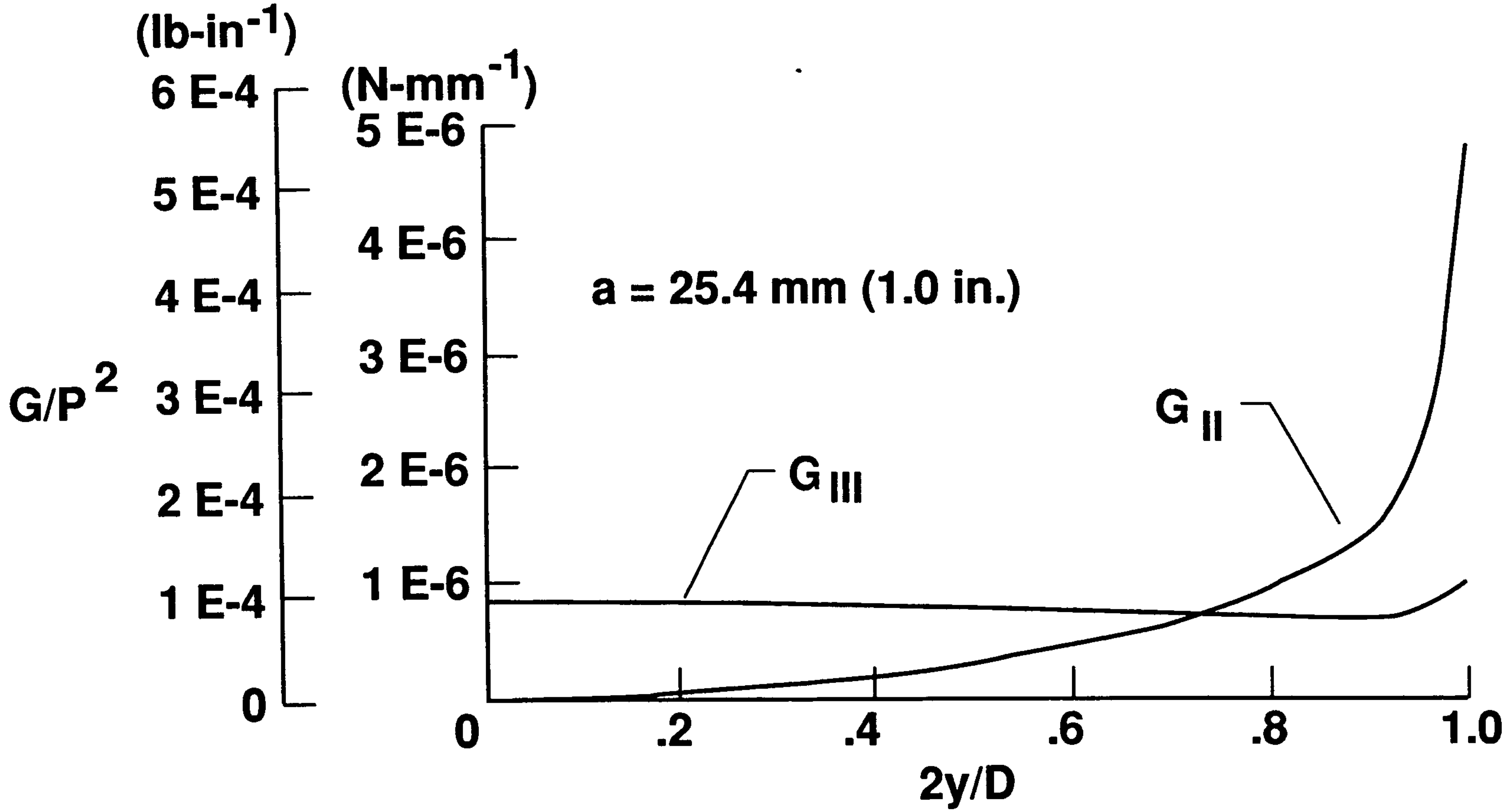

Figure 13a - G_{II} and G_{III} Distribution Along Delamination Front, S2/SP250, D = 12.7 mm (0.5 in.), a = 25.4 mm (1 in.)

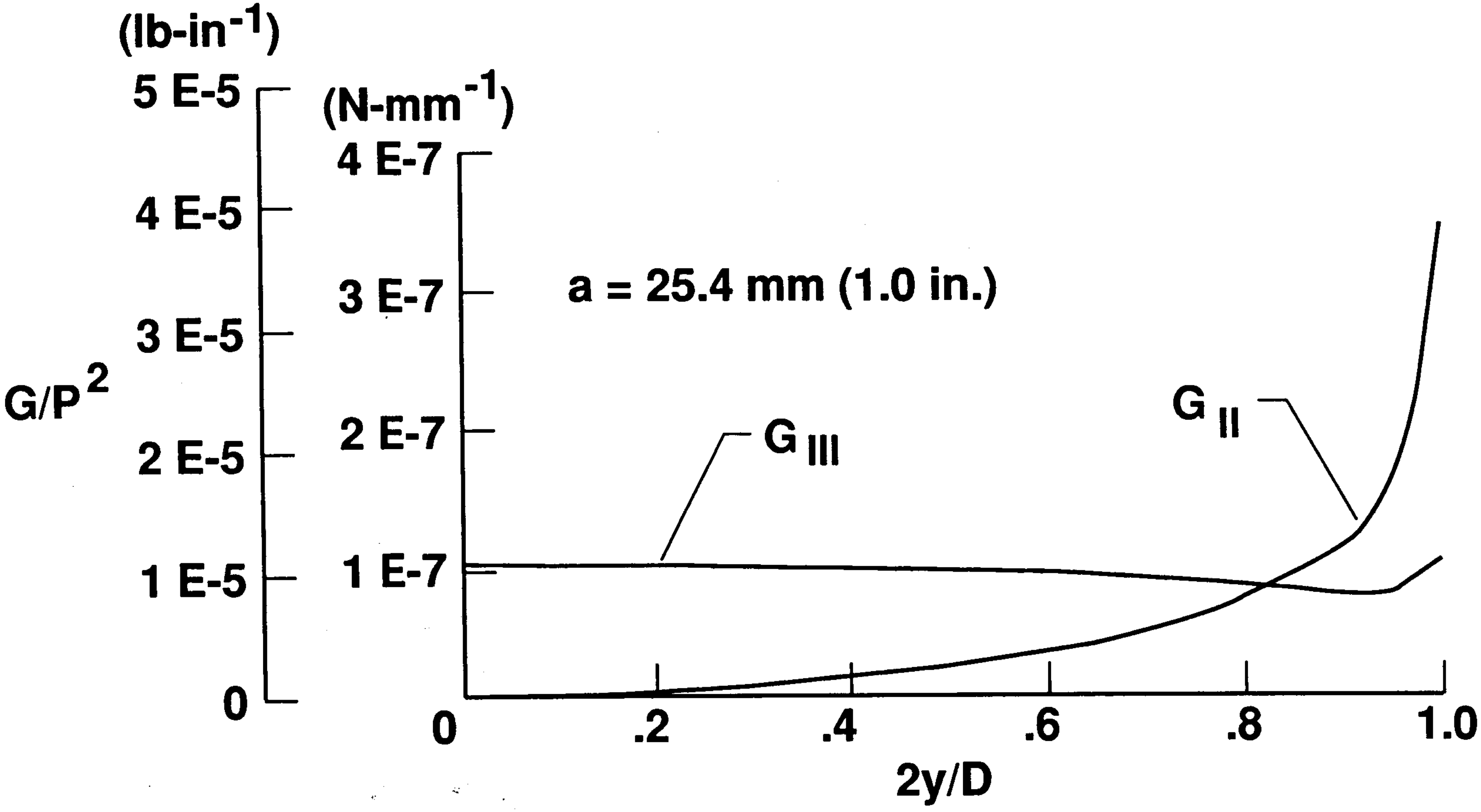

Figure 13b - G_{II} and G_{III} Distribution Along Delamination Front, S2/SP250, D = 25.4 mm (1 in.), a = 25.4 mm (1 in.)

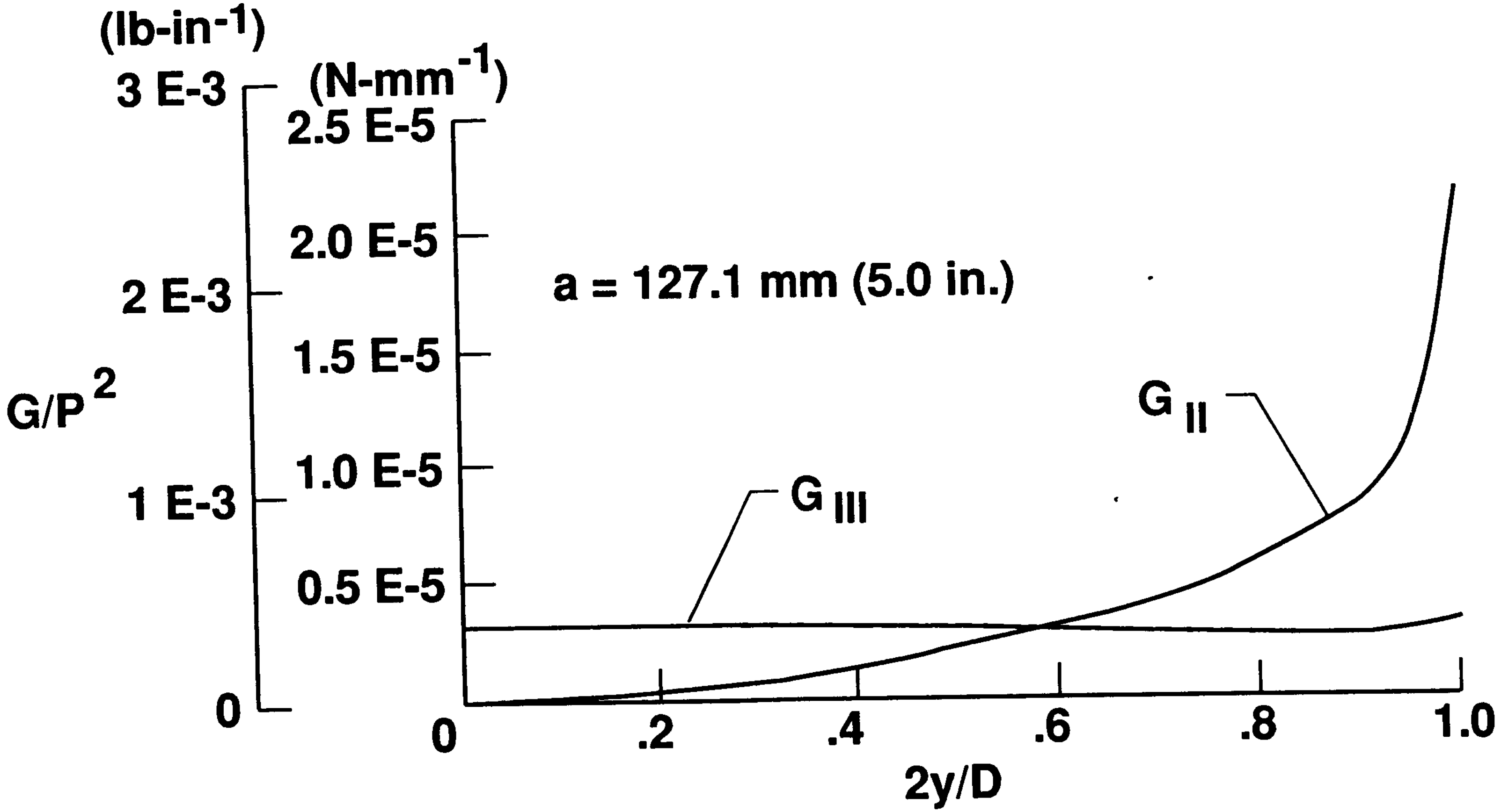

Figure 14a - G_{II} and G_{III} Distribution Along Delamination Front, AS4/3501-6, D = 12.7 mm (0.5 in.), a = 127.1 mm (5 in.)

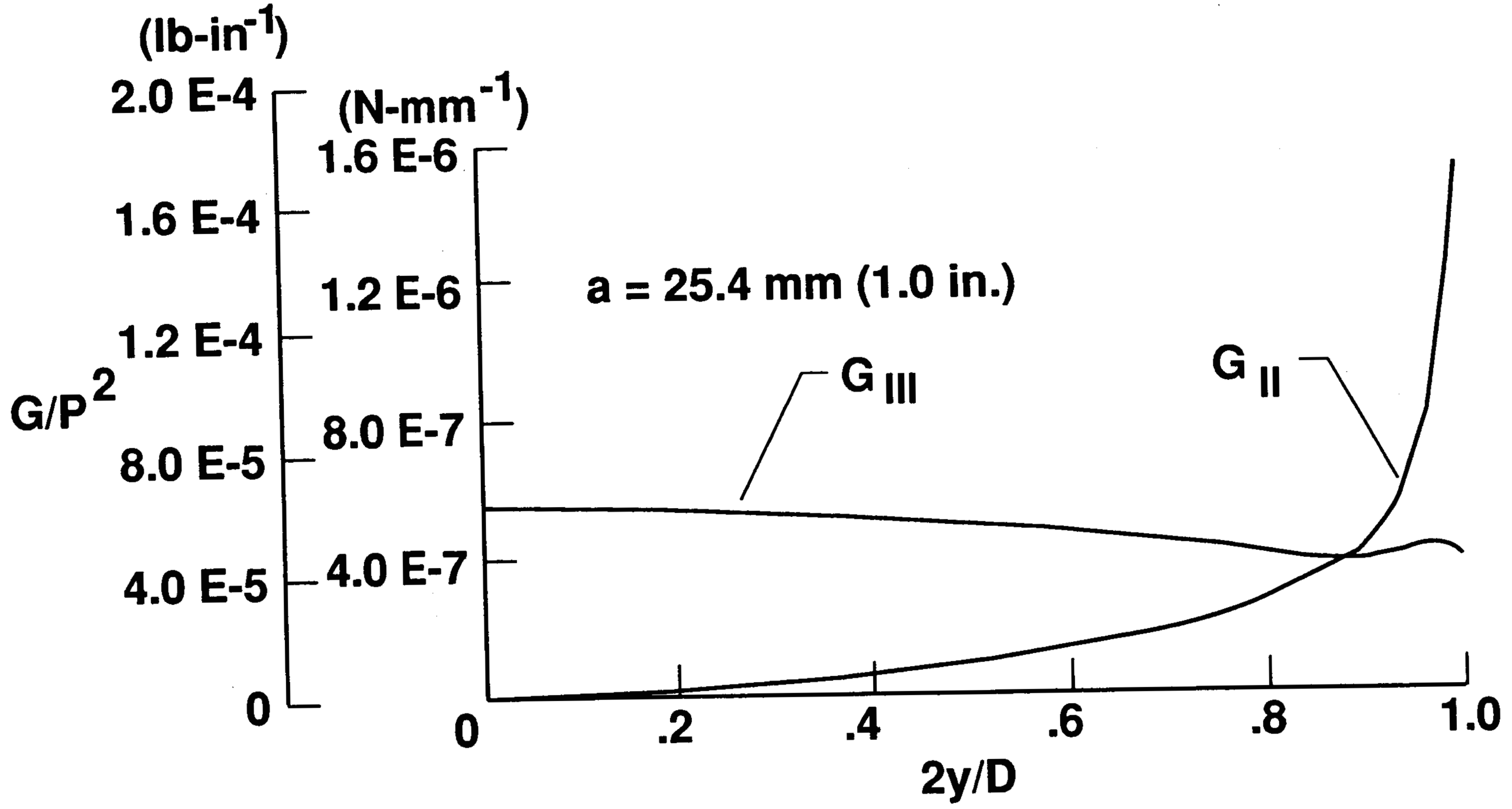

Figure 14b - G_{II} and G_{III} Distribution Along Delamination Front, AS4/3501-6, D = 12.7 mm (0.5 in.), a = 25.4 mm (1 in.)

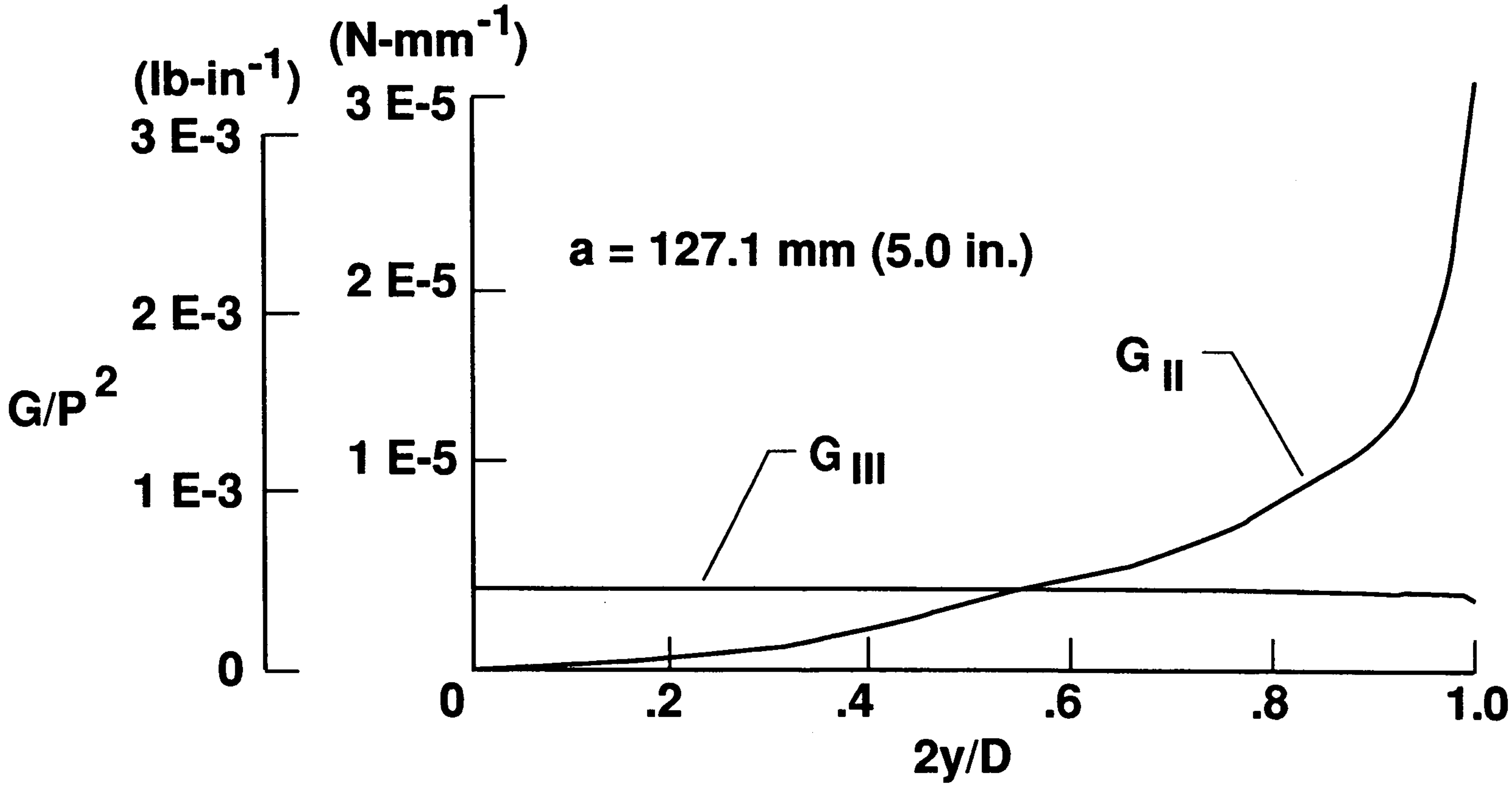

Figure 15a - G_{II} and G_{III} Distribution Along Delamination Front, Aluminum Alloy and AS4/3501-6, D = 12.7 mm (0.5 in.), a = 127.1 mm (5 in.)

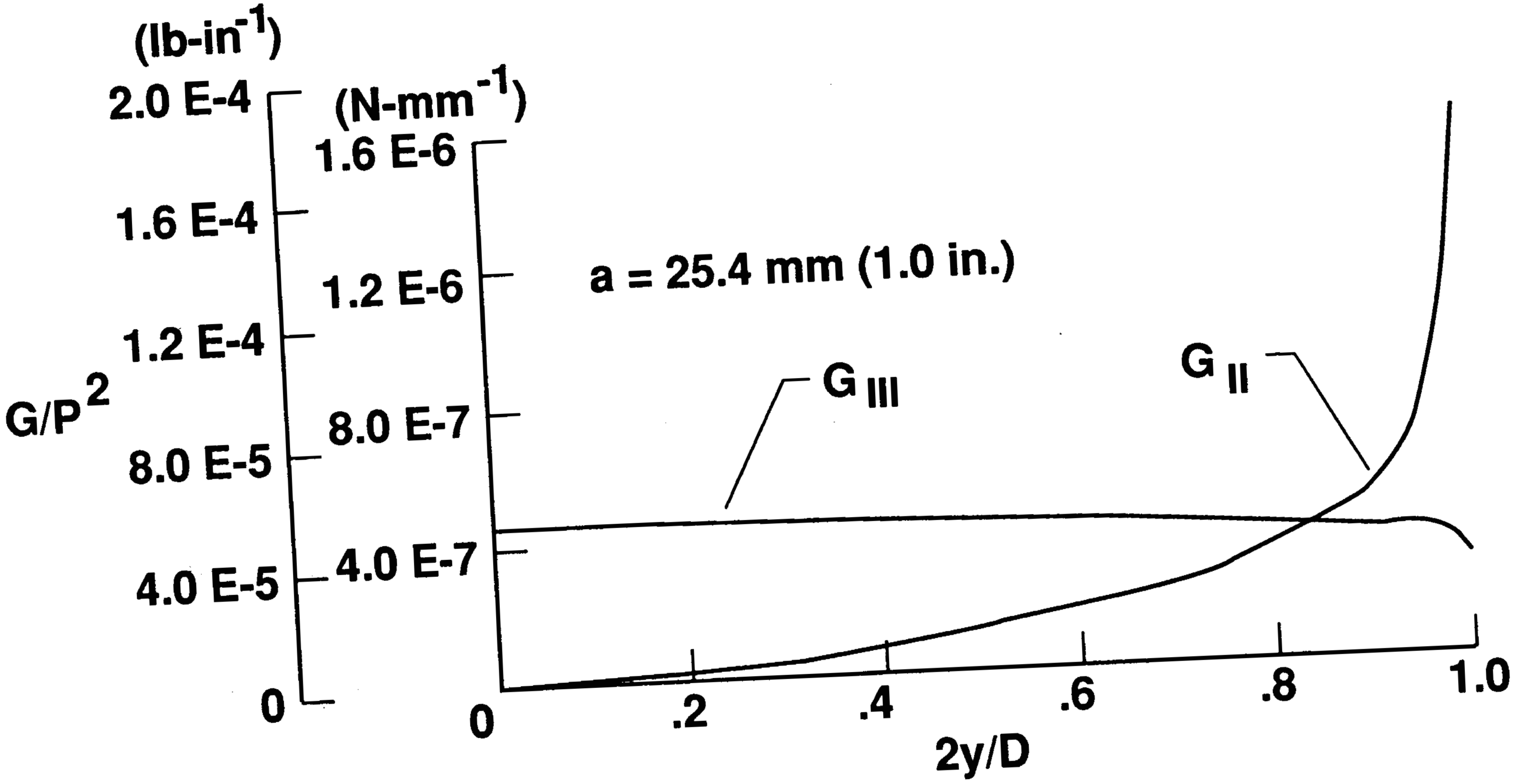

Figure 15b - G_{II} and G_{III} Distribution Along Delamination Front, Aluminum Alloy and AS4/3501.6, D = 12.7 mm (0.5 in.), a = 25.4 mm (1 in.)

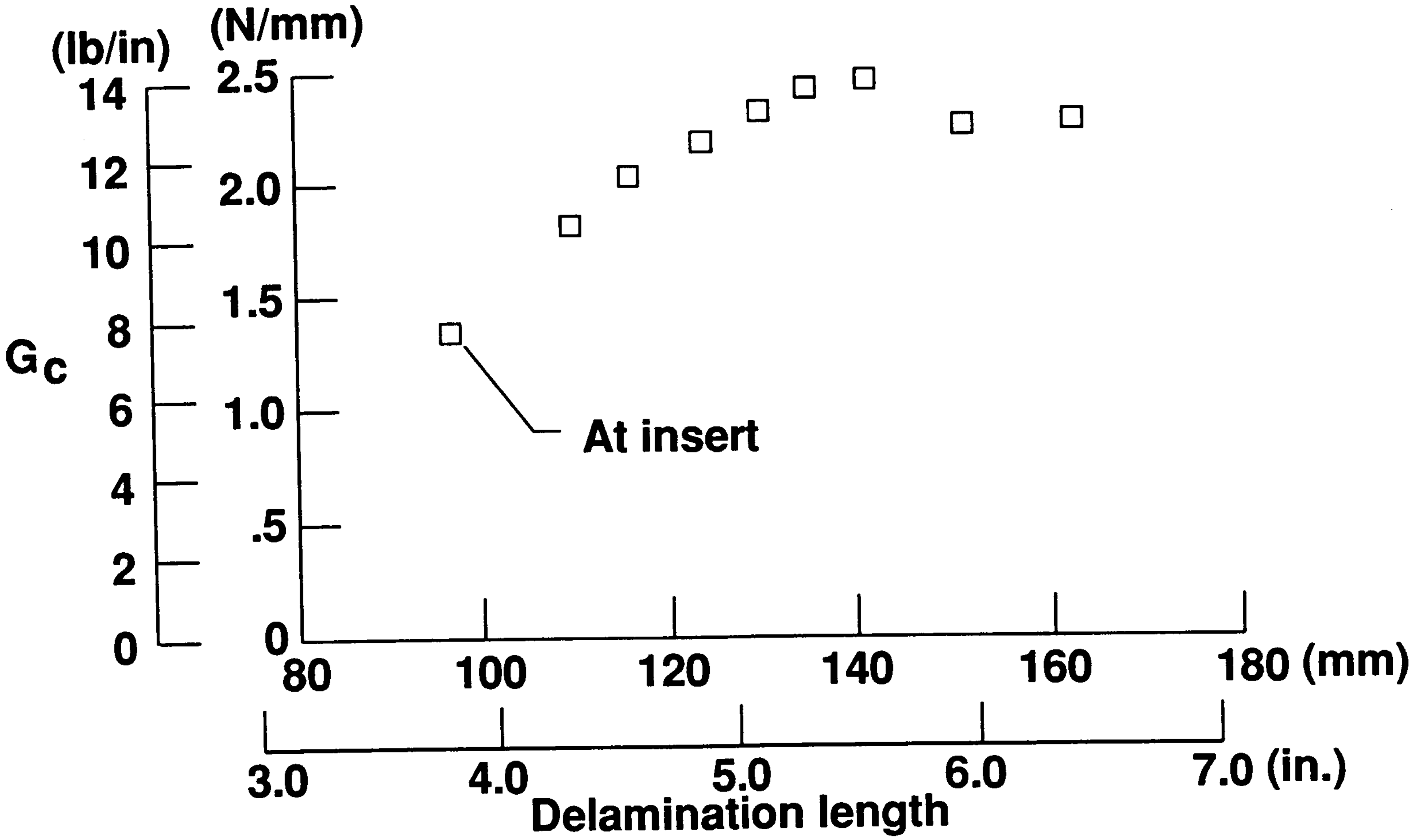

Figure 16 - G_c Versus Delamination Length, S2/SP250, D = 25.4 mm. (1.0 in.)

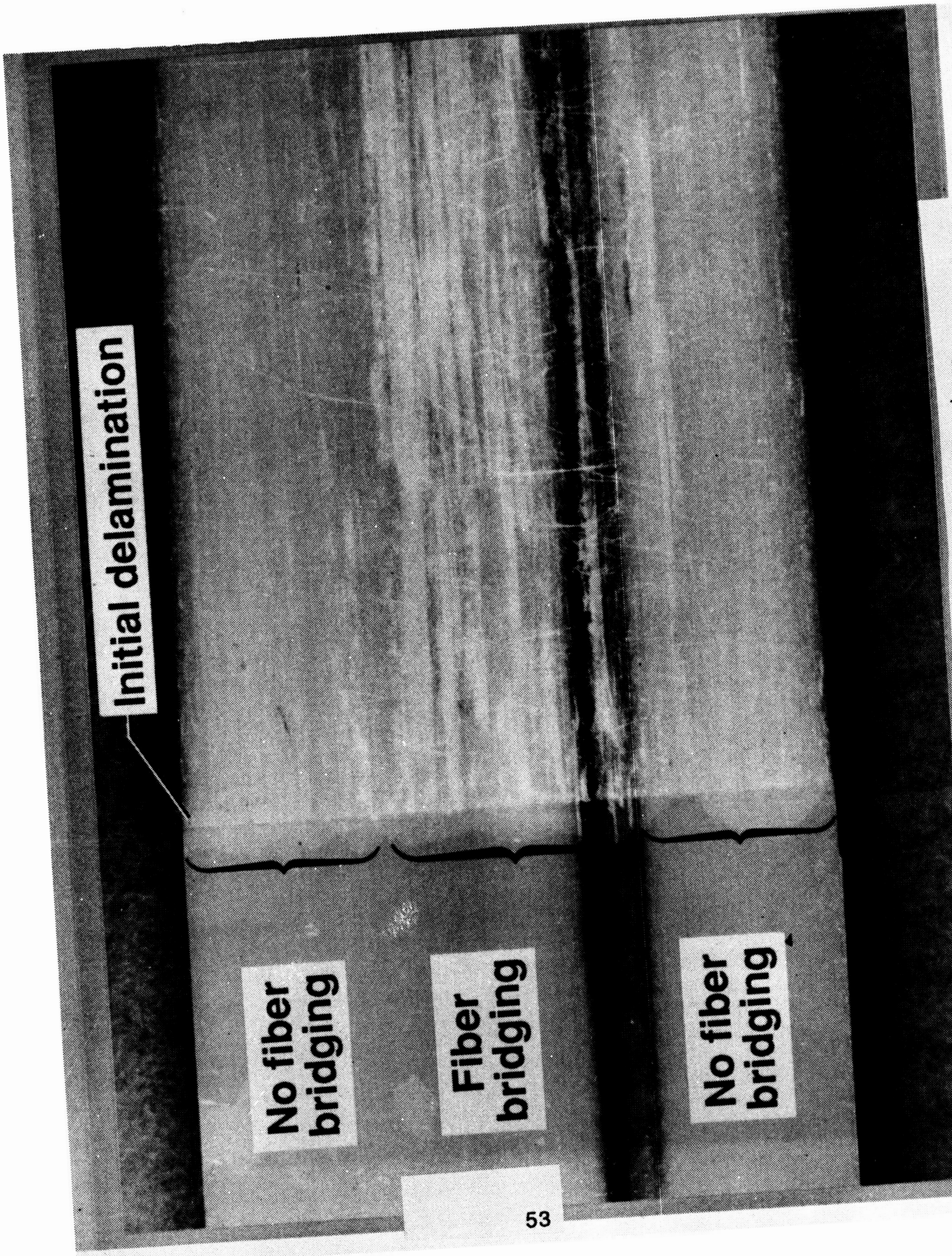

Figure 17 - Fracture Surface of SCB Specimen

ORIGINAL PAGE IS
OF POOR QUALITY

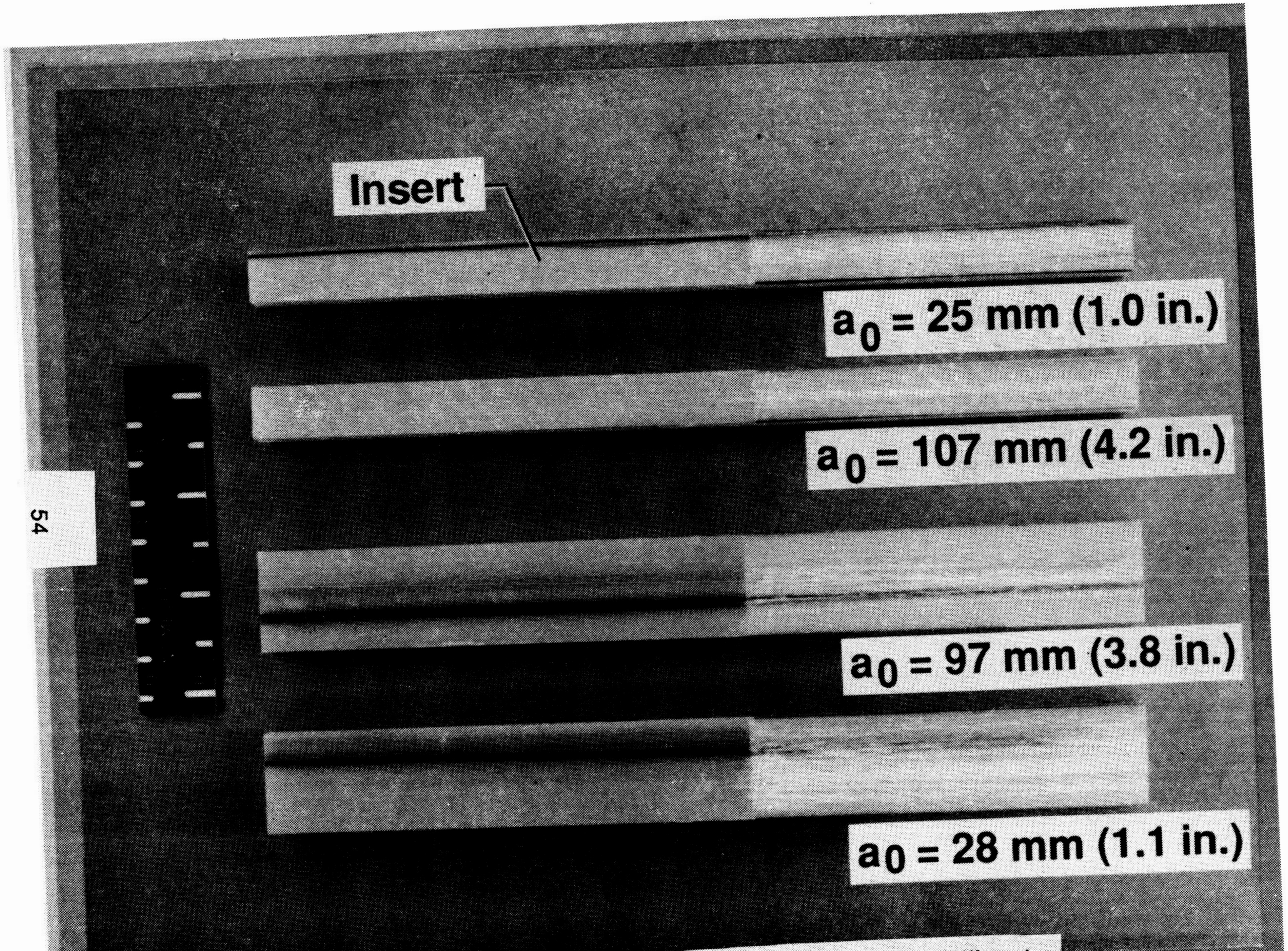

Figure 18 - Fracture Surfaces of SCB Specimens with Different Initial Delamination Lengths

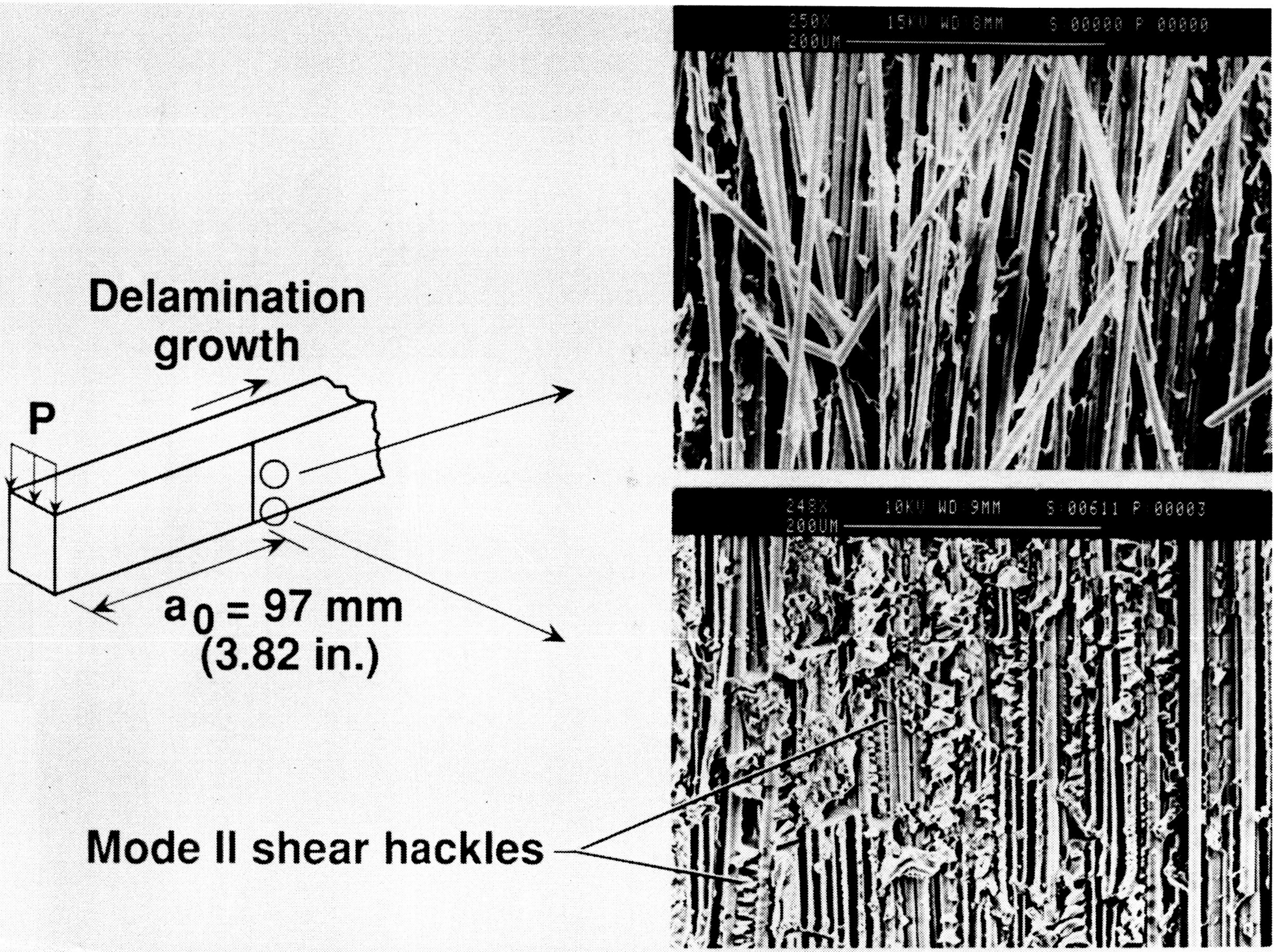

Figure 19 - Micrograph of Fracture Surface

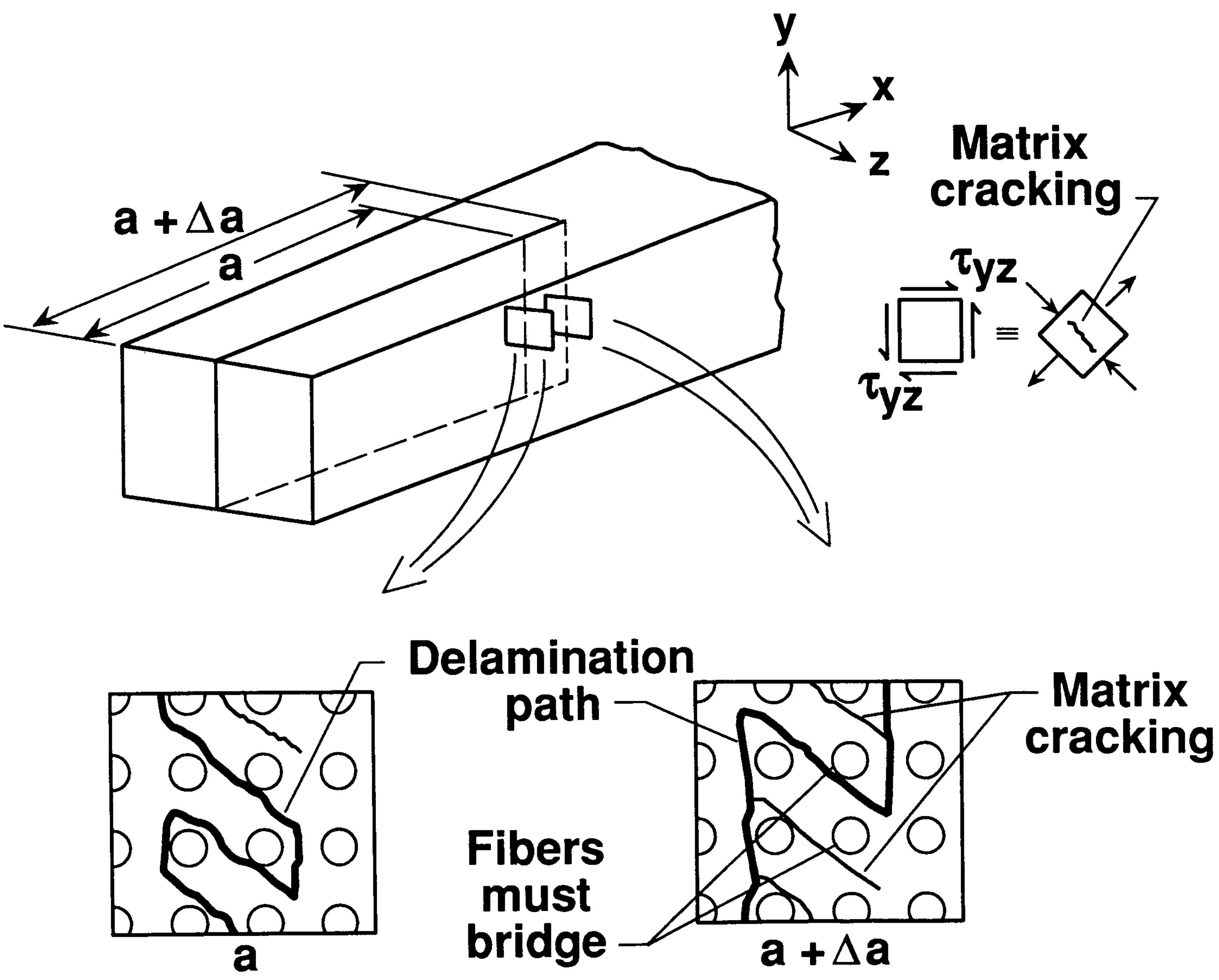

Figure 20 - Schematic of Mode III Fiber Bridging

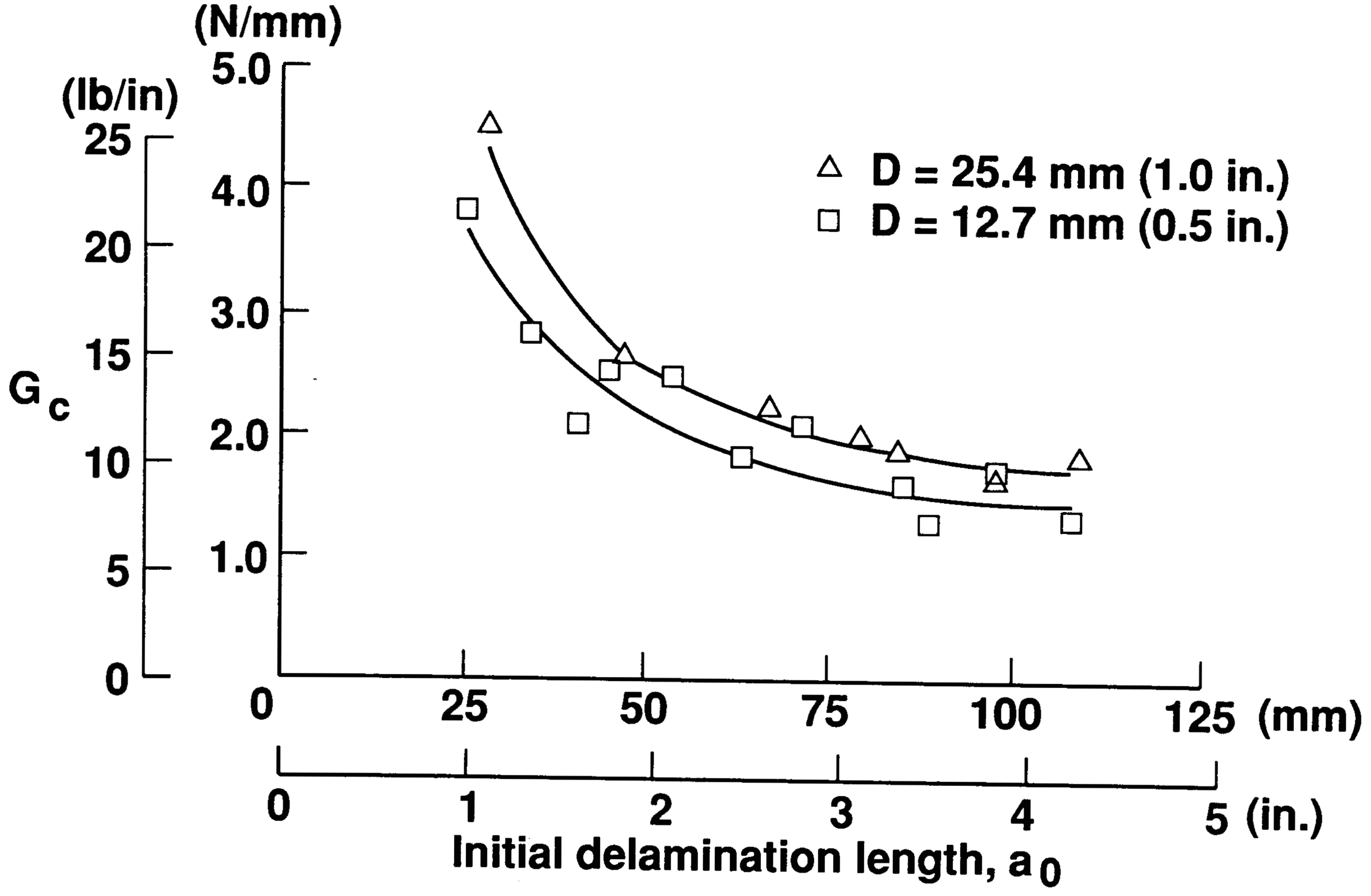

Figure 21 - Variation of G_c with Initial Delamination Length

National Aeronautics and Space Administration

Report Documentation Page

1. Report No. NASA TM-101562	2. Government Accession No.	3. Recipient's Catalog No.

4. Title and Subtitle

Evaluation of the Split Cantilever Beam For Mode III Delamination Testing

5. Report Date

March 1989

6. Performing Organization Code

7. Author(s)

Roderick H. Martin*

8. Performing Organization Report No.

10. Work Unit No.

505-63-01-05

9. Performing Organization Name and Address

NASA Langley Research Center,
Hampton, VA 23665-5225

11. Contract or Grant No.

13. Type of Report and Period Covered

Technical Memorandum

12. Sponsoring Agency Name and Address

National Aeronautics and Space Administration
Washington, DC 20546-0001

14. Sponsoring Agency Code

15. Supplementary Notes

*National Research Council Research Associate at Langley Research Center

16. Abstract

A test rig for testing a thick split cantilever beam for scissoring delamination (mode III) fracture toughness was developed. A 3-D finite-element analysis was conducted on the test specimen to determine the strain energy release rate, G, distribution along the delamination front. The virtual crack closure technique was used to calculate the G components resulting from interlaminar tension, G_I, interlaminar sliding shear, G_{II}, and interlaminar tearing shear, G_{III}. The finite-element analysis showed that at the delamination front no G_I component existed, but a G_{II} component was present in addition to a G_{III} component. Furthermore, near the free edges, the G_{II} component was significantly higher than the G_{III} component. The G_{II}/G_{III} ratio was found to increase with delamination length but was insensitive to the beam depth. The presence of G_{II} at the delamination front was verified experimentally by examination of the failure surfaces. At the center of the beam, where the failure was in mode III, there was significant fiber bridging. However, at the edges of the beam where the failure was in mode III, there was no fiber bridging and mode II shear hackles were observed. Therefore, it was concluded that the split cantilever beam configuration does not represent a pure mode III test. The experimental work showed that the mode II fracture toughness, G_{IIc}, must be less than the mode III fracture toughness, G_{IIIc}. Therefore, a conservative approach to characterizing mode III delamination is to equate G_{IIIc} to G_{IIc}.

17. Key Words (Suggested by Author(s))

Composite material
Delamination
Mode III
Fracture Toughness
Split Cantilever Beam
Strain energy release rate

18. Distribution Statement

Unclassified - Unlimited
Subject Category - 39

19. Security Classif. (of this report)	20. Security Classif. (of this page)	21. No. of pages	22. Price
Unclassified	Unclassified	58	A04

NASA FORM 1626 OCT 86